- Master Thesis -

The effect of oxic degradation on organic temperature proxies: A case study from the coastal shelf off Honshu Island, Japan

submitted by
Frederike Wittkopp

December 2012

Royal Netherlands Institute for Sea Research (NIOZ)
University of Utrecht, Faculty of Geosciences

1^{st} Supervisor: Prof. Dr. ir. S. Schouten
2^{nd} Supervisor: Dr. G.-J. Reichart

Statement of originality of the MSc Thesis

I declare that this is an original report which is entirely my own work. Where I have made use of the ideas of other writers, I have acknowledged the source in all instances. Where I have used any diagram or visuals I have acknowledged the source in all instances. This report has not and will not be submitted elsewhere for academic assessment in any other academic course.

Student Number: 3618307

Utrecht, December 2012

Contents

Abstract

Organic temperature proxies provide powerful tools to reconstruct past sea surface temperatures. An important requirement for those proxies is their stability towards diageneis. The most prominent diagenenic process is oxic degradation of organic matter, which is a selective process and degrades compounds at different rates. As proxies mostly comprise ratios of different compounds, different degradation rates of the individual compounds involved will lead to a bias of proxy based sea surface temperatures. Thus it is important to know how the composition of biomarkers varies in terms of oxic degradation and the possible impacts on organic temperature proxies, i.e. $U^{K'}_{37}$, LDI and TEX_{86}. To draw constraints on the impact of oxic degradation on those organic proxies, surface sediments and four cores underneath the oxygen minimum zone off Honshu Island (Japan) were analyzed. Regarding the effect of oxic degradation on the organic carbon and biomarker concentrations in the sediment it was observed, that the concentrations increased where the oxygen concentrations of the overlying waters were low and the following order of resistance towards oxic degradation was established: TOC $>$ alkenones $>$ GDGTs. Sea surface temperature reconstructions with LDI could not be established, because diols were detected in only low amounts. An increase in $U^{K'}_{37}$ and therefore in temperature is found for the surface sediments with high oxygen concentrations in the overlying water column, resulting in an overestimation of sea surface temperatures of 5.5 °C. The likely cause for this increase is the preferential degradation of the $C_{37:3}$ alkenone. BIT values are slightly higher in the oxic environment than in the suboxic environment, suggesting preferential preservation of the continental

derived GDGTs under oxic conditions. While TEX_{86}^{H} seemingly is not affected by oxic degradation, the application of TEX_{86}^{L} lead to an underestimation of sea surface temperatures up to 6 °C, when the sediment samples are located in the range of 0 m to 1000 m water depth. This is probably due to differential abundances of GDGT-3 above and below 1000 m water depth. The study demonstrates, that individual degradation rates within a compound class can occur and thus bias the sea surface temperature towards higher temperatures. It is therefore essential to know the oxygenation history of the study area when those proxies are applied, especially reconstructions based on $U_{37}^{K'}$. TEX_{86}^{L} needs to be appplied with caution, when the water depth of the sediment is above 1000 m.

1. Introduction

1.1. Biomarker Lipids

Sedimentary organic matter (OM) in the oceans experiences contribution from mainly two sources: the terrestrial and the marine environment. Higher plant debris is transported by rivers to the ocean and is deposited on the continental slope. Those higher land plants are characterized by, amongst others, a lower C/N ratio and by the abundance of specific organic geochemical compounds such as lignin and leaf waxes (Meyers, 1997). Although those are very prominent characteristics and despite the large input of 0.4×10^{15} g C yr^{-1} it is difficult to detect substantial amounts of terrestrial organic matter in the oceans (Hedges et al., 1997). Thus, the largest source of sedimentary organic matter is the detrius of phytoplankton. As primary producer, phytoplankton mainly depend on light and nutrient availability, has a high net production in terms of growth rates and reproduction and thus contributes more to the sediment than organisms with higher trophic levels (Killops and Killops, 2005). However, in the marine realm light penetrates only tens of meters deep and continental weathering increases the concentration of the essential biolimiting nutrients, nitrogen and phosphorus, on shelf seas resulting in different production rates within the system (Meyers, 1997; Killops and Killops, 2005).

The OM that escaped nutrient recycling in the surface layer sinks down the water column and undergoes decomposition during settlement (Meyers, 1997, and references therein). The molecular composition of fresh organic matter, listed in general order of abundance, consists of proteins, carbohydrates, nu-

cleic acids and lipids. Nucleic acids, carbohydrates, proteins are relatively easy biodegradable while most lipids are preserved in the sediment. Lipids can provide information about the source organisms that produced those lipids. This is the base for the so called biomarker principle. Biomarkers are compounds preserved in the sediment, that can be linked to specific organisms because they are the only organisms producing those compounds. For example high abundances of isorenieratene, which is a characteristic pigment produced by green sulphur bacteria, indicate past photic zone euxinia (Menzel et al., 2002) or dinosterol, which is mainly produced by dinoflagellates, indicates the presence of this algal group (Killops and Killops, 2005).

1.2. Organic Proxies

To assess past climate conditions, proxies are used. Proxies are based on preserved fossil remains, which contain information on past environmental or oceanographic processess. Information about sea surface temperatures can be, for example, provided by the Mg/Ca ratio in planktonic foraminifera: magnesium is incorporated into the tests more easily with increasing temperatures (Nurnberg et al., 1996; Elderfield and Ganssen, 2000). The δ^{18}O record provided by foraminifer reflects not only sea surface temperatures, but also global ice volume and local salinity (Shackleton, 1982, 1987). For the δ^{18}O record it becomes difficult to disentangle the different influences. Carbonate dissolution is a problem that affects foraminiferal proxies and leading to gaps in the record because target organisms got dissolved, i.e. during shoaling of the calcite compensation depth (CCD) and low pH in the oceans during the PETM (Zachos et al., 2005, 2007).

Another way to assess paleo environments is measuring the distribution of biomarker lipids. As required for biomarkers, their production must be limited to a few, preferably known, organisms. Furthermore, they should be ubiquitous and with that cover a wide temperature range. Organic proxies are generally

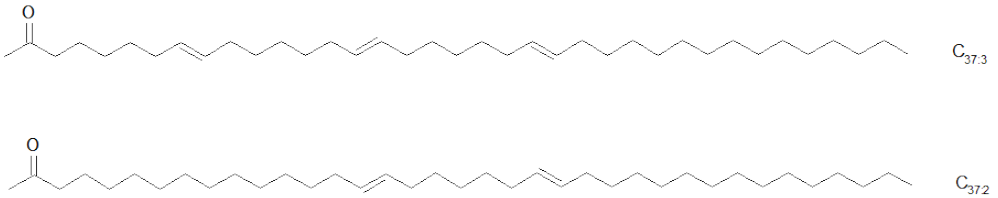

Figure 1.1.: Structure of long-chain alkenones used for the $U_{37}^{K'}$ proxy

calibrated with core tops of sediments to establish a correlation between the distribution of those lipids and sea surface temperature (SST) of the overlying waters, e.g. Müller et al. (1998), Kim et al. (2008), Kim et al. (2010). Brassel et al. (1986) proposed a very powerful tool for SST reconstructions, the U_{37}^{K} index based on the degree of unsaturation in C_{37} alkenones derived from haptophytes (Fig. 1.1). Until today, the biological function of those alkenones is still unknown. Prahl and Wakeham (1987) introduced a modified version of this index, the $U_{37}^{K'}$ and a calibration for this proxy based on laboratory cultures of *Emilana huxleyi*. Müller et al. (1998) then introduced a revised equation derived from global core top calibaration, with an calibration error of 0.05 U_{37}^{K} units, corresponding to 1.5 °C.

$$U_{37}^{K'} = \frac{[C_{37:2}]}{[C_{37:2} + C_{37:3}]}$$

$$U_{37}^{K} = 0.033T + 0.043$$

$$U_{37}^{K'} = 0.033T + 0.044$$

The production depth of alkenones is restricted to the penetration depth of light. This depth is variable, ranging from 10 m to 120 m, but the best correlation between alkenones and temperature has been established for the first 10 m of the water column (Müller et al., 1998; Ohkouchi et al., 1999). Müller

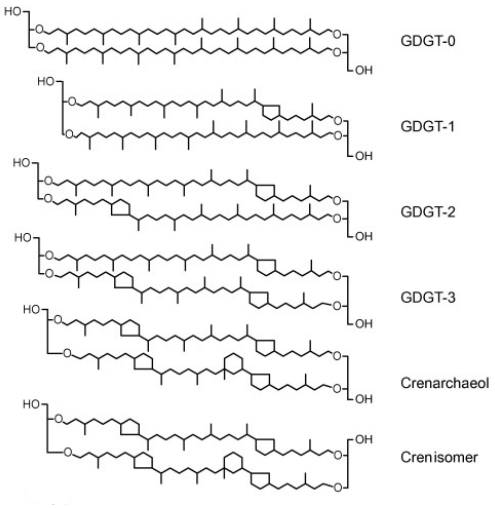

Figure 1.2.: Overview of GDGT structures, Lengger et al. (2012)

et al. (1998) also assumed that the alkenone derived SST reflects the annual mean except in regions where phytoplankton growth season is short, such as the subpolar regions, although a strong correlation with seasonal temperatures has been reported for several other regions (i.e. Sikes et al. (2005); Yamamoto et al. (2007); Versteegh et al. (2007); Leider et al. (2010)).

Another approach to reconstruct SST is the use of glycerol dibiphytanyl glycerol tetraethers (GDGTs) introduced by Schouten et al. (2002). These GDGTs are specific membrane building blocks of marine archaea which distribution is depending on the surrounding temperature, and carry different amounts (0–4) of cyclopentyl moieties. A special GDGT is crenarchaeol which additionally carries a cyclohexyl moiety (Figure 1.2). TEX_{86} is a SST proxy based on the relative abundance of GDGTs preserved in the sediment. For an improved reconstruction, Kim et al. (2010) introduced the TEX_{86}^{L} (low temperature) and TEX_{86}^{H} (high temperature). TEX_{86}^{L} is more suited for the SST reconstruction of (sub)polar oceans than previously TEX_{86}. TEX_{86}^{H}, which is the log of TEX_{86}

was calibrated with data of temperate and tropical oceans. Kim et al. (2010) suggests to apply TEX_{86}^{H} to subtropical, tropical and former greenhouse world oceans. The calibration error of TEX_{86}^{H} is ±2.5 °C (Kim et al., 2010). In contrast to TEX_{86}^{H} GDGT-3 and the regio isomer of crenarchaeol have been excluded for TEX_{86}^{L}. TEX_{86}^{H} not only includes GDGT-3 in the numerator but also the crenarchaeol regio isomer. The threshold for the application of TEX_{86}^{H} is SST >15 °C, as below this threshold TEX_{86}^{H} overestimates the sea surface temperature. Although showing a larger error (±4 °C), TEX_{86}^{L} is giving a better estimation than TEX_{86}^{H} of sea surface temperatures below <15 °C (Kim et al., 2010). Although GDGTs are produced throughout the whole water column, several studies have shown that TEX_{86} likely reflects temperatures of the upper 100 m of the water column (Wuchter et al., 2005, 2006). Because of their efficient packaging into larger sinking particles, GDGTs from the photic zone reach the bottom much faster than the deeper produced GDGTs due to the absence of grazers and the related aggregates (Wuchter et al., 2005, 2006). TEX_{86} is correlated with mean annual SST, although a bias to seasonal temperature has been reported for several regions (Kim et al., 2008; Herfort et al., 2006; Schouten et al., 2002).

$$TEX_{86}^{L} = \frac{GDGT-2}{GDGT-1+GDGT-2+GDGT-3}$$

$$SST(^{\circ}C) = 67.6 \times log\left(TEX_{86}^{L}\right) + 46.9$$

$$TEX_{86}^{H} = \frac{GDGT-2+GDGT-3+cren-isomer}{GDGT-1+GDGT-2+GDGT-3+cren-isomer}$$

$$SST(^{\circ}C) = 68.4 \times log\left(TEX_{86}^{H}\right) + 38.6$$

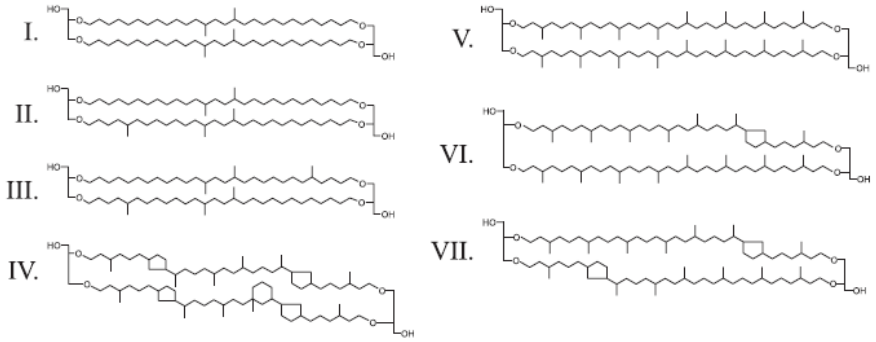

Figure 1.3.: Strucutres of soil derived, branched GDGTs (Hopmans et al., 2004)

$$BIT = \frac{[I + II + III]}{[I + II + III] + [IV]}$$

Sinninghe Damsté et al. (2000) first discovered non-isoprenoidal GDGT lipids in peats, lake and coastal sediments. These branched GDGTs are probably produced by some Acidobacteria living in the anoxic part of soils (Weijers et al., 2011; Sinninghe Damsté et al., 2011; Weijers et al., 2006a), and are characterized by a different degree of methylation (4 to 6 methyl groups) and different number (0-2) of cyclopentane moieties (Fig. 1.3). Soil derived isoprenoid GDGTs can bias the TEX_{86} proxy (Weijers et al., 2006b), therefore the BIT (Branched versus Isoprenoid Tetraether index) must be calculated to determine relative contribution of GDGTs from soils (Hopmans et al., 2004). The BIT index expresses the abundance of branched GDGTs and crenarchaeol in soils and sediments. In marine environments, BIT is high (i.e. 0.9) close to river mouths, but decreases to 0 with increasing distance from the shore (Hopmans et al., 2004; Weijers et al., 2006b).

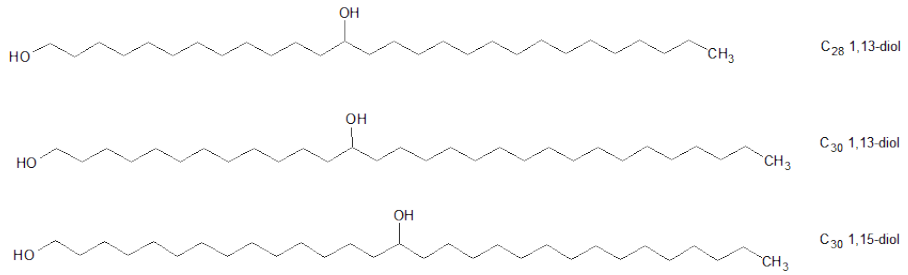

Figure 1.4.: Structure of long chain diols building up the LDI

The most recent proxy is the LDI (Long-chain Diol Index) based on long-chain diols, which have been first discovered by de Leeuw et al. (1981) (Fig. 1.4). Versteegh et al. (2000) tested the long chain diols as a tool for tracing past sea surface temperatures, since the composition of diols showed variations matching changes in contemporary sea surface temperatures and the glacial-interglacial cyclicity. Eustigmatophyte algae are known to produce these compounds (Volkman et al., 1992). However it is questionable if they are the sources, since these algae are rarely reported in the marine environment, while diol distributions of cultured eustigmatophytes are not comparable to the distribution in marine environments (Rampen et al., 2012, and references therein). By analyzing the fractional abundance of C_{30} and C_{28} diols in surface sediments from different settings, Rampen et al. (2012) found a strong negative correlation for the relative abundance of C_{28} and C_{30} 1,13-diols with SST. In addition, the C_{30} 1,15-diol shows a strong positive correlation with mean annual SST. The calibration with SST yields a correlation of mean annual SST of the first 30 m with an calibration error of 2 °C (Rampen et al., 2012).

$$LDI = \frac{[C_{30}1,15]}{[C_{28}1,13 + C_{30}1,13 + C_{30}1,15]}$$

$$LDI = 0.033T + 0.095$$

Diagenesis during sedimentation and burial can potentially change the proxy ratios giving an error in SST estimates. Diagenesis in geochemical terms includes processes that affect the composition of organic matter. Those processes can, amongst others, involve oxidation, defuctionalization and aromatisation. Oxic degradation is the most prominent process and the effect of oxygen on the preservation of OM will be discussed in more detail in section 1.3.

1.3. Influence of oxygen on the preservation of organic matter

It has been a long and controversial discussion whether oxygen has an influence on organic matter degradation, (i.e. Lee (1992); Hartnett et al. (1998); Hedges et al. (1999, and references therein)). A very complex mixture of factors, such as sedimentation rates, the flux of organic carbon, bottom water oxygen concentrations and primary productivity govern the preservation/degradation of organic matter in the ocean. Primary productivity, sedimentation rate and oxygen concentrations play the most important roles. Oxygen concentrations in the water column are less important, since the residence time of organic matter at the seafloor is much longer than in the water column. Thus, oxygen concentrations at the sediment-water interface and in the sediment itself are more important. By studying the organic matter content on the Washington continental slope, Hedges et al. (1999) pointed out the importance of oxygen exposure time. In example, the organic carbon to surface area ratio decreased with increasing distance from the slope and increasing oxygen exposure time. The oxygen exposure time increases due to lower sedimentation rain rates and thus decreased burial efficiency. As a consequence, the OM is exposed longer to oxygen and thus more degraded. Demonstrating the effect of post-depositional oxidation, Hoefs et al. (1998a) reported an OM loss of nearly 80% in oxidized samples compared to the unoxidized part of a turbidite and attributed this to

the post-depositional penetration of oxic bottom-waters. They also reported a drastic change in the biomarker composition: For example, compared to the unoxidized part, the oxidized part of the core shows a drastic drop in isoprenoid alkane and alkene concentrations, but an increase in *n*-alkanes. They also observed a selective preservation of aliphatic biomacromolecules under oxic conditions. Sinninghe Damsté et al. (2002) assessed the influence of oxygen on OM preservation, especially on biomarkers, by investigating sediments in the oxygen minimum zone (OMZ) of the Arabian Sea. Oxygen minimum zones are helpful to study because they provide sites with oxic and oxygen-depleted bottom waters close to each other and thus both sites experience the same surface water productivity. Differences in the composition of the sedimentary organic matter due to primary productivity can be ruled out and oxygen is the main determining factor. By chosing three different sites, one just in the OMZ, one just below and another one well below the OMZ, they observed prominent differences in the biomarker composition: Steroids are less resistant towards oxic degradation than alkenones and alkyl diols which in turn are less resistant than terrestrial *n*-alkanes. From this they concluded that the biomarker composition changes with oxygen exposure time and paleoenvironmental reconstructions should be done with caution. These findings are also consistent with the results of Hoefs et al. (2002) who established a general order of resistance for the Madeira Abyssal Plain (MAP) turbidites: *n*-alkanes>diols/keto-ols>alkenones>steroids.

Sinninghe Damsté et al. (2002) do not find an alteration of the $U_{37}^{K'}$ by preferential degradation of the $C_{37:3}$ alkenone which is in line with findings of Madureira et al. (1995), Teece et al. (1998) and Prahl et al. (1989). A preferential degradation of this alkenone would lead to a shift in the $U_{37}^{K'}$ ratio and therefore to an over estimation of sea surface temperatures (Prahl et al., 1988). Hoefs et al. (1998a) did observe a preferential degradation of the $C_{37:3}$ alkenones in the oxidized part of turbidites compared to the $C_{37:2}$ alkenone. Already a low degree of selective degradation, with a degradation ratio (DR) between 1 and 1.5 leads to an error in temperature estimations that are beyond

the analytical error of 0.5 °C (Hoefs et al., 1998b). Zabeti et al. (2010) reported a marine bacteria, *Dietzia maris* sp. S1 which seems to selectively degrade the di- and tri-unsaturated alkenone and thus causing a bias towards warmer sea surface temperatures. It is assumed that the additional double bond of the $C_{37:3}$ gives the alkenone a higher reactivity (Hoefs et al., 1998b). Shifts in $U_{37}^{K'}$ have also been reported by Hoefs et al. (1998b), Gong and Hollander (1999), Huguet et al. (2009), Kim et al. (2009b) and Zabeti et al. (2010). Whether the $U_{37}^{K'}$ is affected by this phenomenon of preferential $C_{37:3}$ degradation might be a reflection of the bacteria population at the sampling site (Hoefs et al., 1998b; Zabeti et al., 2010, and references therein), since some studies do not report such preferential degradation.

Only few of degradation studies included GDGTs. Yamamoto et al. (2012) reported for their sediment trap study constant TEX_{86} values throughout the water column and from that concluded that TEX_{86} is not affected by degradation during settling.

For crenarchaeol and GDGT-0, Sinninghe Damsté et al. (2002) reported a relatively high preservation efficiency, but it is not less prone to oxic degradation than other lipids. Schouten et al. (2004) examined the effect of redox conditions on the TEX_{86} and found that TEX_{86} differed only within the analytical error (TEX$\pm$0.02) in sediments deposited under different redox conditions. Kim et al. (2009b) exposed sediment samples from the Namibian upwelling region to three contrasting redox conditions, testing the stability of TEX_{86}. Statistical analysis showed no significant differences between the samples permeable for bacteria and a control sample in an air-tight bag. Huguet et al. (2009) reported no bias of TEX_{86} under oxic bottom-waters as long as the concentrations of soil derived isoprenoid GDGTs are low. Continental derived isoprenoid GDGTs can bias TEX_{86} since terrestrial organic matter is preferentially preserved over marine organic matter, thus input of corresponding GDGTs from the continental realm will bias TEX_{86} towards colder or warmer temperatures. For turbidites from the Madeira Abyssal Plain, this phenomenom can lead to a bias ranging from

−6 °C to 2 °C of todays SST (Huguet et al., 2008, 2009). The stability of TEX_{86} might be due to the preferential degradation of functional groups by bacteria. The functional groups are the same for all GDGT structures and thus all are supposed to be affected in the same rate.

For the LDI, no studies were carried out yet. Ferreira et al. (2001) found sharp drops in diol concentrations, especially for the C_{30}-1,15 diol, in Mediterranean sapropels and attributed this to post-depositional oxidation. Decreased concentrations in oxic environments for long-chain diols are also reported by Hoefs et al. (2002) and Sinninghe Damsté et al. (2002). Sun and Wakeham (1994) calculated low degradation rates for long-chain diols, suggesting a high stability in anoxic environments. Unfortunately, these studies investigated only the total C_{28}-C_{32}-diol concentrations, so that the differential behavior of the LDI-diols remains unknown.

1.4. Aim of Study

Although many degradation studies included $U^{K'}_{37}$, TEX_{86} rarely has been studied and LDI not at all. The extend of a potential bias caused by oxic degradation on these proxies is often not well constrained. To gain insight in this, the degradation of biomarker lipids and organic proxies in the very pronounced oxygen minimum zone off Honsu Island was examined. To this end the impact on TEX_{86}, $U^{K'}_{37}$ and LDI proxies were investigated in surface sediments and four sediment cores exposed to a range in oxygen concentrations. The research will provide constraints on the impact of oxic degradation on these organic proxies.

2. Study Area

2.1. Hydrography of coastal northeast Japan

The coast of northeast Japan is dominated by three major surface currents (Figure 2.1): the Oyashio Current, the Kuroshio Current and the Tsugaru Warm Current (TWC). The Kuroshio current splits in two at the south western tip of central Japan. One branch flows along the Japanese east coast, the other branch enters the East/Japan Sea via the Korean/Tsushima Strait (KTS) and exits the East Sea via the Tsugaru Strait as the TWC. The TWC sills at a depth of 130 m into the Pacific Ocean where it overlays the cold waters of the Oyashio Current (Chang et al., 2004; Shibahara et al., 2007). The Kuroshio Current is a part of the wind-driven subtropical gyre circulation cell and transports warm ($\geq$15 °C) (Fig. 2.2), saline and oligotrophic waters from the south along the north eastern coast of Japan (Oba et al., 2006). As a western component of the Kamchatka-Alaskan Current the Oyashio Current transports cold (usually $<$14 °C), less saline and nutrient-rich waters along the coast of Hokkaido. An oxygen minimum zone (OMZ) exists in the intermediate waters of the Oyashio region, probably due to high surface productivity and poor intermediate-water ventilation (Ohkushi et al., 2003; Shibahara et al., 2007). The mixing front, characterized by sharp salinity and temperature gradients, is situated around 37-39°N but it shifts with season. Around October, the boundary is located at 40°N and moves to 41.5°N in December (Shibahara et al., 2007; Oba et al., 2006; Hagino et al., 2005). But the intensity of the two currents and therefore their mixing front is also strongly dependent on the atmosphere: two pressure cells,

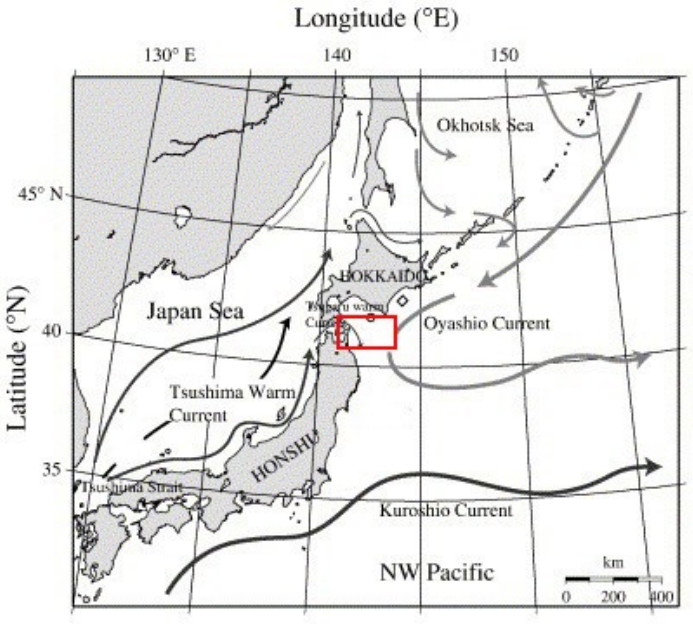

Figure 2.1.: Location map of the three dominating currents in the NW Pacific, (Hoshiba et al., 2006)

the Aleutian Low and the Okhotsk High pressure cells determine the northward or southward shift of the two currents (Harada et al., 2012; Oba et al., 2006). In the past, the two currents shifted to the north or to the south respectively, due to climate change (Oba et al., 2006).

The northern Pacific's marginal seas play an important role for the ventilation of the intermediate waters. Nowadays, the North Pacific Intermediate Water (NPIW) is characterized as a salinity minimum around 26.8 σ_θ at a depth between 300–800 m (Shibahara et al., 2007; Ikehara et al., 2006; Ohkushi et al., 2003). However, the fundamental processes of the formation of the NPIW are unclear (Keigwin, 1998). There are two different theories about the origin of the NPIW. The first theory is based on the assumption that the Okhotsk Sea is the source region of the NPIW. The intermediate water is produced by

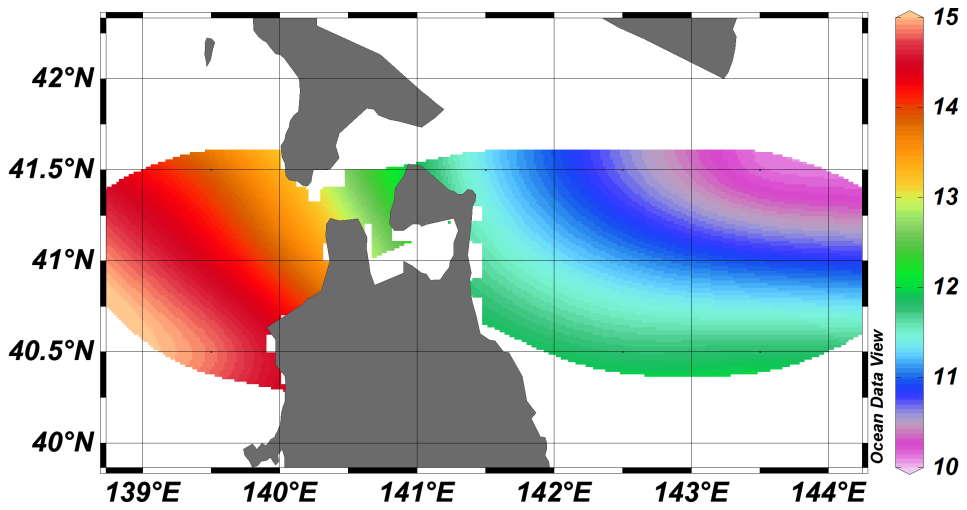

Figure 2.2.: Annual surface temperature for NE Japan (World Ocean Atlas, 2009)

brine rejection during sea ice formation in the Okhotsk Sea. These low saline waters diffuse downwards along the subpolar gyre and therefore ventilate the NPIW. Since the water was not in contact with the atmosphere, it already is characterized by significant lack in oxygen. The oxygen content decreases further away from the source and is recognizable as a distinct OMZ in the central and northeast Pacific (Keigwin, 1998).

The second theory assumes that the NPIW is formed at the Kuroshio-Oyashio mixing front since this region contains the newest NPIW that is formed in the Pacific. This theory also assumes that the oxygen concentration decreases away from the source (Keigwin, 1998). Keigwin (1998) came to the conclusion that the Okhotsk Sea plays an important role for the NPIW independently from the two theories. The Okhotsk Sea definitely provides the source water for the Oyashio Current and possibly provides also the source water for the NPIW. Thus, changes in the Okhotsk Sea affect and have affected NPIW and

its ventilation. Thereby, the intensity of the OMZ is coupled to ventilation changes in the Okhotsk Sea (Ohkushi et al., 2003).

Several paleoceanographic studies have been carried out on the oxygenation history of the OMZ, intermediate and bottom waters, by interpreting foraminiferal assemblages in the northeast Pacific covering the timespan from the Last Glacial Maximum (LGM) to present day (Shibahara et al., 2007; Ikehara et al., 2006; Ahagon et al., 2003; Ohkushi et al., 2003; Keigwin, 1998). During the LGM, intermediate waters originated from the Bering Sea, due to brine rejection, and were well ventilated as well as the bottom waters (Shibahara et al., 2007; Ohkushi et al., 2003; Keigwin, 1998; Ikehara et al., 2006). This changed in the Bølling/Allerød (B/A) period: The ventilation of the intermediate waters decreased, probably due to upwelling triggered by changes in the thermohaline circulation (Shibahara et al., 2007). This had also an influence on the local OMZ which was strengthened and probably most intense during the B/A. Also the oxygen concentrations of the bottom water was at a minumum during the B/A (Shibahara et al., 2007; Ikehara et al., 2006; Ahagon et al., 2003). The situation became restored during the Younger Dryas (YD). In the Holocene the ventilation of the Pacific switched to the contemporary situation and NPIW production started (Ohkushi et al., 2003). The early Holocene was characterized by high oxygen concentrations in bottom waters and a well developed OMZ (Ikehara et al., 2006; Ohkushi et al., 2003), which changed again in the mid Holocene to a weak OMZ. Because less sea ice is formed today, the brine rejection decreased as well and therefore the important mechanism for the NPIW ventilation also becomes weakened, which leads to a well developed OMZ and low oxygen concentrations in the bottom waters (Shibahara et al., 2007; Ikehara et al., 2006; Ohkushi et al., 2003).

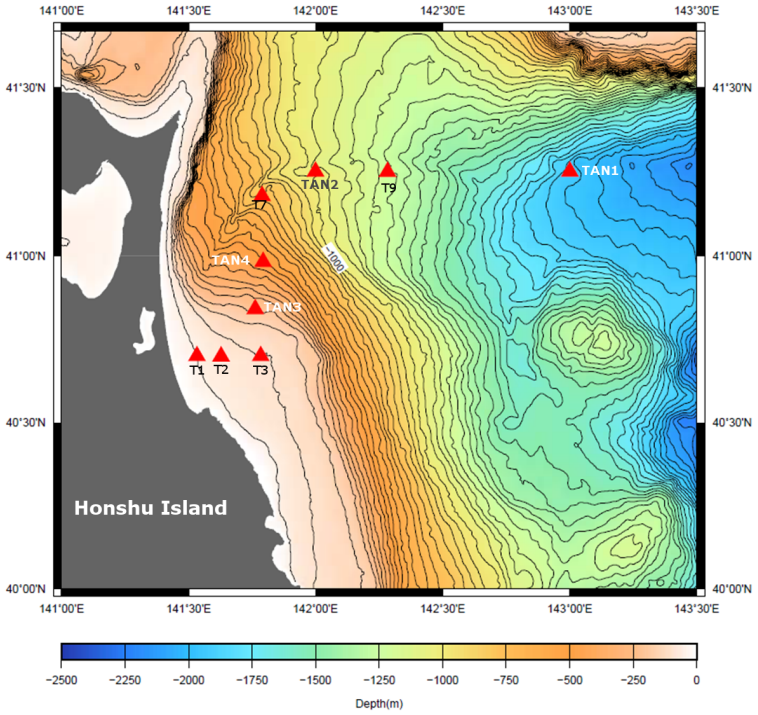

Figure 2.3.: Bathymetric Map of sampling area (courtesy JAMSTEC)

2.2. Characteristics of Study Area

The sediment cores and surface sediments analyzed in this project were taken underneath the pronounced OMZ off Honshu Island (Figure 2.3), Japan. In contrast to many other OMZ, the top of this OMZ shows a gradual decrease in oxygen concentrations (Tab. 2.1, Fig. 2.4) over a large depth interval and thus is located much deeper in the oceanic water column than other OMZs. The studied area is influenced by the outflowing waters of the Tsugaru Strait, the TWC and to some extend by the Oyashio Current.

Table 2.1.: Overview of sampled stations (degree, decimal minutes), samples and oxygen concentrations (DO).

Station	Sample Type	Core length	Latitude	Longitude	Water Depth (m)	DO [ml/l]
T1	Surface		40°41.989 N	141°31.990 E	55	
T2	Surface		40°41.982 N	141°37.669 E	81	
T3	Surface		40°42.041 N	141°47.027 E	105	
TAN3	Core	20 cm	40°50.415 N	141°45.677 E	202	5.5
TAN4	Core	20 cm	40°58.891 N	141°47.572 E	482	2.5
T7	Surface		41°10.6472 N	141°47.348 E	760	
TAN2	Core	20 cm	41°15.003 N	142°00.028 E	1046	0.7
T9	Surface		41°14.9118 N	142°16.8429 E	1250	0.7
TAN1	Core	20 cm	41°14.918 N	142°59.989 E	1938	1.4

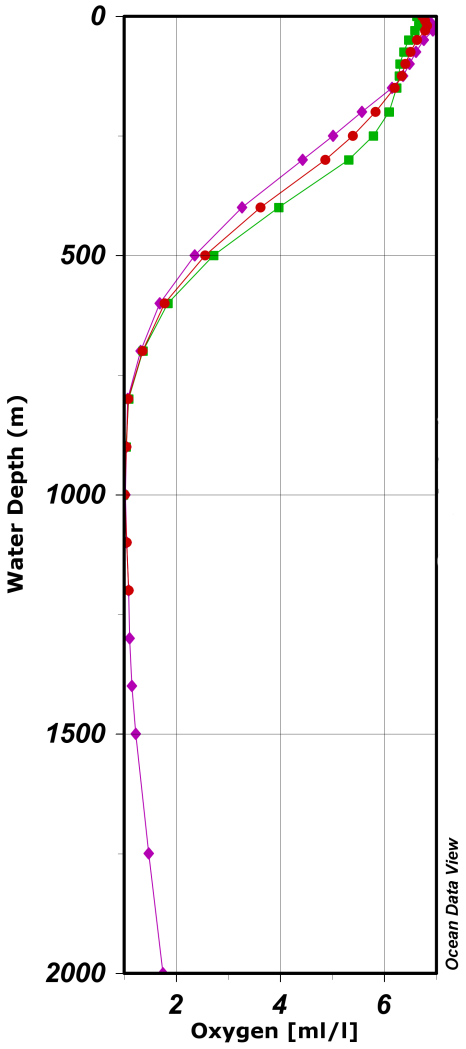

Figure 2.4.: Oxygen concentrations of the study area, representing the cruise transect: 41.5°N, 141.5(purple line)/142.5(red line)/143.5(green line)°E (World Ocean Atlas, 2009)

3. Methods

3.1. Sample Preparation

The cores were recovered during a research cruise on board the R/V Tansei-maru from 21^{st} to 25^{th} of August 2011. First, the cores were sliced on board: The first two centimeter were sliced in $0.5\,cm$ intervals, followed by $1\,cm$ intervals for the following two to ten centimeters, the last ten centimeters were then sliced in $2\,cm$ intervals. As surface sediment samples served a $2\,cm$ thick slice from the other cores. After the arrival, the samples were freeze dried and ground by using mortar and pestle.

3.2. Oxygen Measurements

Undisturbed cores recovered from 500, 1000 and 2000 m depth were on board incubated for seven hours. The incubator was set to the temperatures and O_2 concentrations at the respective sites. After incubating the cores, O_2 concentrations were measured with a microelectrode (OX-50, Unisense).

3.3. Sample Workup

To analyze total organic carbon (TOC) and bulk δ^{13}C of organic matter, $10\,mg$ to $15\,mg$ of sediment samples were decarbonated with 2N HCl and subsequently were washed with bidistilled water until pH$\approx$7 prior to analysis on the Organic Elemental Analyzer. For biomarker analysis, sediments ($2\,g$ to $9\,g$)

were extracted using an Accelerated Solvent Extractor (ASE) (Dionex 350) at 100 °C and a pressure of 1.03×10^6 Pa using a mixture of dichloromethane (DCM)/methanol (MeOH) (9:1, v/v). The total lipid extract (TLE) was separated using an Al_2O_3 column, subsequently eluted with hexane:DCM (9:1, v/v), hexane:DCM (1:1, v/v) and DCM:methanol (1:1, v/v). For the analysis of GDGTs, the polar fraction (DCM:MeOH) was concentrated under N_2, dissolved in hexane:iso-propanol (99:1, v/v) and filtered through a $0.4\,\mu m$, 4 mm-diameter PTFE filter before injection into a high pressure liquid chromatography/mass spectrometer (HPLC/MS). An internal standard of $0.1\,\mu g$ C_{46} GDGT was added. The ketone fraction (hexane:DCM, 1:1) was dissolved in Ethyl Acetate (EtoAc). $0.221\,ng$ of a C_{19} ketone was added as an internal standard to the fraction. Diols were analyzed by sylilating the polar fraction with $10\,\mu l$ pyridine, $10\,\mu l$ N,O-bis(trimethylsilyl) trifluoroacetamide (BSTFA) and $5\,\mu l$ EtoAc and heating the mixture in an oven for 20 minutes at 60 °C. As an internal standard, $2.58\,\mu g$ of a C_{22} 7,16-diol was added. Both ketones and diols were analyzed by gas chromatography (GC) and gas chromatography/mass spectrometer (GC/MS).

3.4. Biomarker analysis

Bulk analysis was performed with a Thermo Scientific Flash 2000 Organic Elemental Analyser, coupled to an Delta V advantage isotopic ratio-mass spectrometer (IR-MS, Thermo Scientific). Gas chromatography analysis was performed using a Hewlett Packard 6890 chromatograph equipped with an flame ionization detector (FID) and using a silica column CP-Sil 5, 50 mx0.32 mm, film thickness $0.12\,\mu m$. Helium was used as a carrier gas and the oven heated for $20\,°C/min$ from 70 °C to 130 °C followed by a heating rate of $3\,°C/min$ to 320 °C keeping this temperature for $25\,min$. GC/MS analysis was performed on a Thermo Finnigan TraceGC Ultra coupled to a DSQ quadropule mass spectrometer (MS), using a silica column: CP-Sil 5, 25 mx0.32 mm, film thickness

0.12 μm. Helium was used as a carrier gas with a constant flow of 2 ml/min and the oven heated 20 °C/min from 70 °C to 130 °C, continuing with 4 °C/min to 320 °C holding the time for 10 min for the default method, and 25 min for the diol analysis. The long chain diols were analyzed using selected ion monitoring (SIM) of m/z 299, 313, 327, 341 and 355 (Rampen et al., 2012). GDGTs were analyzed using HPLC/APCI-MS Agilent Technologies, following Schouten et al. (2007), equipped with an Prevail Cyano column, 150 mmx2.1 mm. The injection volume was 5 μl. As an eluent, a 9:1 (v/v) mixture of hexane:iso-propanol was used, the flow rate of the mixture was 0.2 ml/min. For increased detection sensitivity, GDGTs were analyzed by using SIM of the $[M+H]^+$ TEX_{86} and BIT GDGTs.

4. Results

4.1. Surface Sediments

4.1.1. TOC

Bulk parameters of the sediments have been measured for all four cores but not for all the surface sediments. The TOC content at the surface is the lowest (<1%) for TAN3, but is relatively constant for the other three stations, with organic carbon contents between 2.5-3% (Fig. 4.1).

4.1.2. Alkenones and $U_{37}^{K'}$

Figure 4.2 shows the abundance of compounds per gram TOC with varying depth. The concentrations of alkenones per gram TOC are almost constantly around $0.5\,\mu g/g$. Alkenones increase in concentration with increasing depth (Figure 4.3). Concentrations of $0.6\,ng/g$ dwt were detected at shallow depths, between 55 m to 200 m. The highest concentration was measured at intermediate depth: $13.5\,ng/g$. At the deeper sampling stations, concentrations decrease again to $10\,ng/g$. Temperatures of 18 °C were reconstructed at the shallowest sampling station and steadily decrease for the other stations down to 14 °C and remain around this temperature.

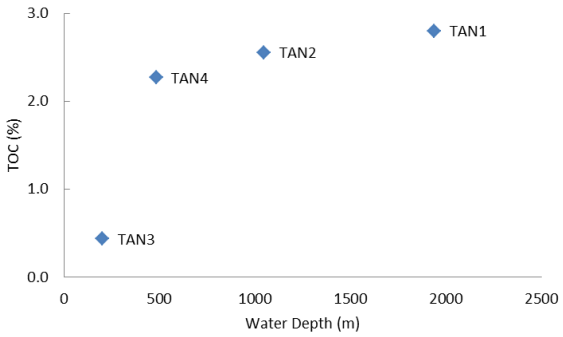

Figure 4.1.: TOC content for surface sediments at 202, 482, 1046 and 1938 m bottom depth

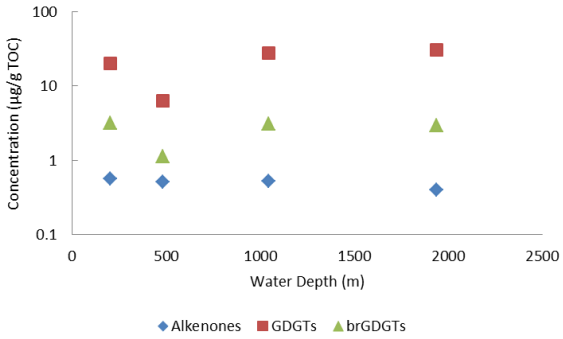

Figure 4.2.: Biomarker concentration in surface sediments normalized to TOC

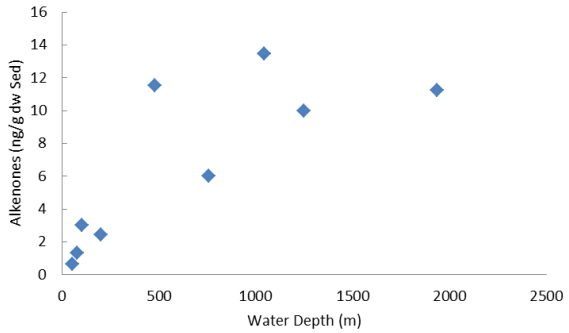

Figure 4.3.: Concentrations of alkenones (ng/g) dw Sed detected in the surface sediments

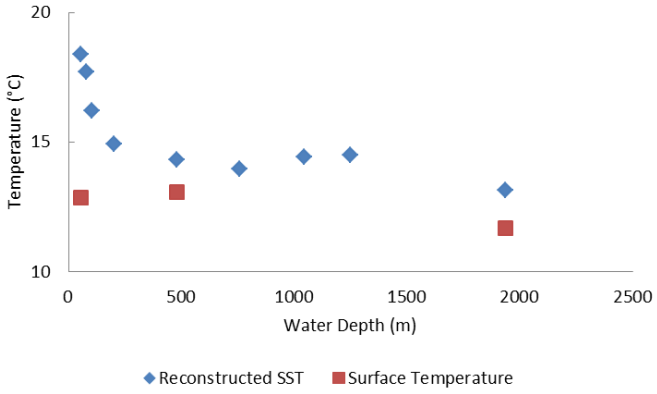

Figure 4.4.: Sea surface temperature reconstructed with $U_{37}^{K'}$ in comparison to surface temperature (Japan Oceanographic Data Center, www.jodc.go.jp).

4.1.3. GDGTs, TEX_{86} and BIT

Figure 4.2 shows the abundance of compounds per gram TOC with varying depth. The concentrations for branched GDGTs are just 10% of those for isoprenoid GDGTs. One exception is TAN4 showing the lowest concentration for both GDGTs. The concentrations of isoprenoid GDGTs increase slowly over the first 1000 m, from $0.2\,\mu g/g$ to $3.4\,\mu g/g$ TOC. The highest concentrations were measured for TAN2, TAN1 and T9, with concentrations ranging from $7.9\,\mu g/g$ to $11\,\mu g/g$ dwt, (Figure 4.5). The concentrations of branched GDGTs follow the trend of isoprenoid GDGTs, but two orders of magnitude lower. At the shallow sampling stations, concentrations are around $0.004\,\mu g/g$ to $0.007\,\mu g/g$, and at the deepest stations around $0.81\,\mu g/g$. The BIT is always well below 0.1, but increased values at shallow depths can be observed: with increasing depths, BIT decreases from 0.06 to nearly 0.01 (Fig. 4.6). TEX_{86}^{H} shows small variations in the reconstructed temperature, with values between 12 °C to 14 °C (Fig. 4.7). TEX_{86}^{L} shows low temperatures for the first 1000 m, with temperatures of 7 °C to 10 °C. Beyond 1000 m depth, TEX_{86}^{L} is in the same range as TEX_{86}^{H}. To assess a potential bias on the TEX_{86} temperatures caused by soil derived GDGTs, the concentrations of crenarchaeol and branched GDGTs were compared to each other (Fig. 4.8). The concentration of crenarchaeol decreases two orders of magnitude with decreasing bottom depth, while the branched GDGTs only decrease one order of magnitude.

4.1.4. Diols

The C_{28} 1,13-diols and in two cases C_{30} 1,13-diols were detected, but the abundances were too low for LDI to be calculated (Fig. 4.9).

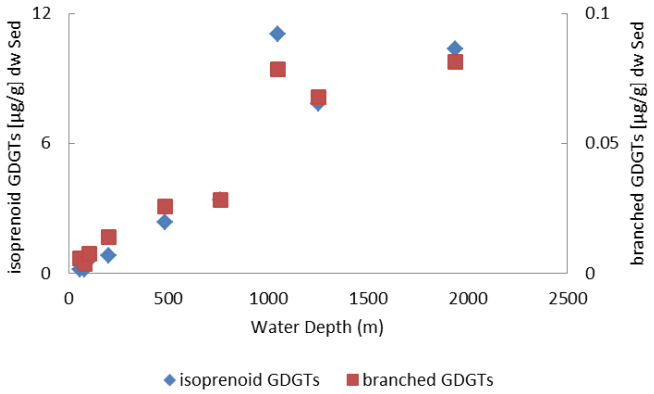

Figure 4.5.: Concentrations of branched and isoprenoid GDGTs (μg/g) dw Sed detected in surface sediments

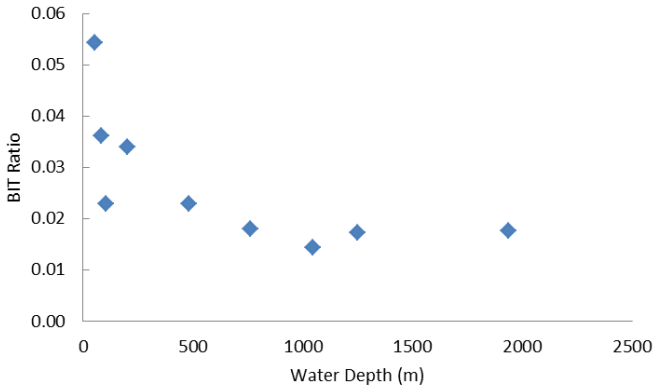

Figure 4.6.: BIT calculated for all surface sediments

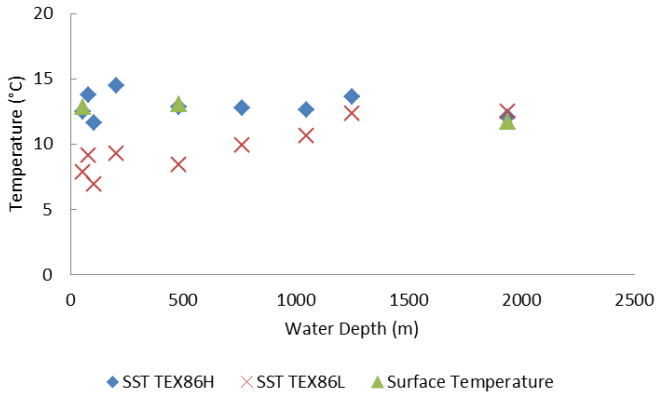

Figure 4.7.: Sea surface temperature reconstructed with TEX_{86}^{H} and TEX_{86}^{L} compared to SST

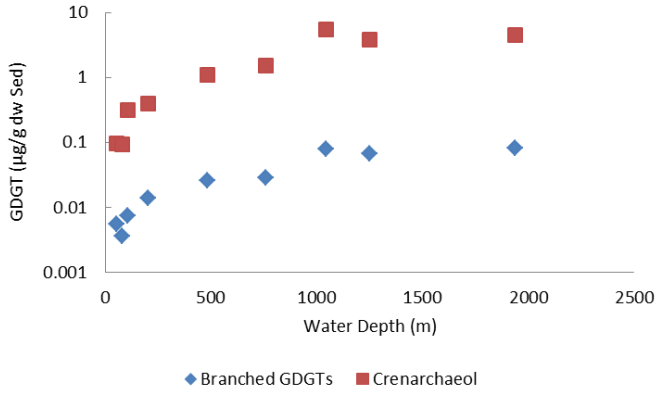

Figure 4.8.: Concentrations of branched GDGTs and crenarchaeol detected in the core top sediments.

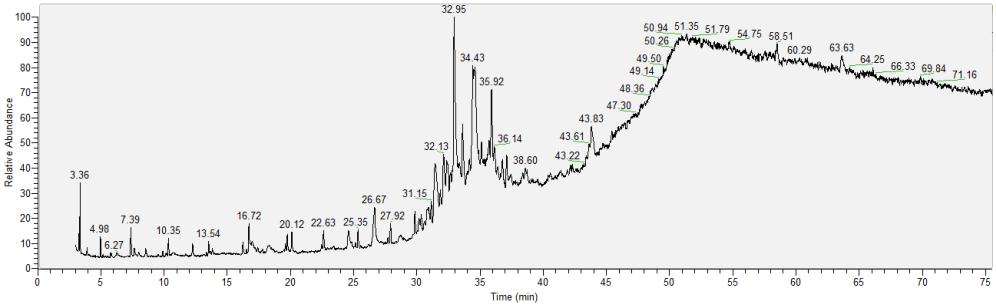

Figure 4.9.: An example SIM chromatogram of TAN1. Diol concentrations where to little to determine LDI

4.2. Cores

4.2.1. Bulk Parameters

The four cores were analyzed for total organic carbon (TOC) and δ^{13}C. The highest TOC values were measured at the surface and values varied between 0.3 and 3%. TAN3 shows the lowest TOC concentrations and TAN2 the most constant values of 2.5-3% (Fig. 4.10). TAN3, TAN4 and TAN1 additionally show a relative decrease of TOC content with depth. Bulk δ^{13}C values range between -22.4 and -21.3‰ for all cores (Fig. 4.11). δ^{13}C decreases with increasing depth, reaching lowest values of -21.4 and -21.2‰ for TAN2 and TAN3 respectively. TAN1 and TAN4 show slightly higher values of -21.8‰.

4.2.2. Alkenone and $U_{37}^{K'}$

The down core analysis of alkenone concentrations revealed a broad scatter in every core (4.12), and no clear trends towards higher or lower concentrations are recognizable. The concentrations, with few exceptions, do not exceed $0.6\,ng/g$ dry weight sediment. The analysis of $U_{37}^{K'}$ shows also a broad scatter with extreme temperature fluctuations between 17 °C to 29 °C (Fig. 4.12). Similar to the concentration profile, no trend towards higher or lower temperature is rec-

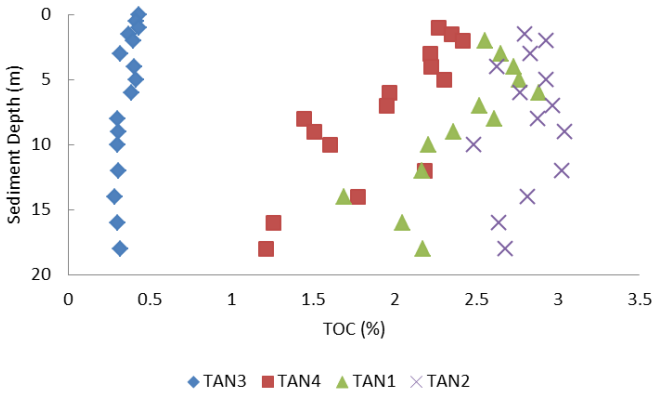

Figure 4.10.: TOC values for all analyzed cores.

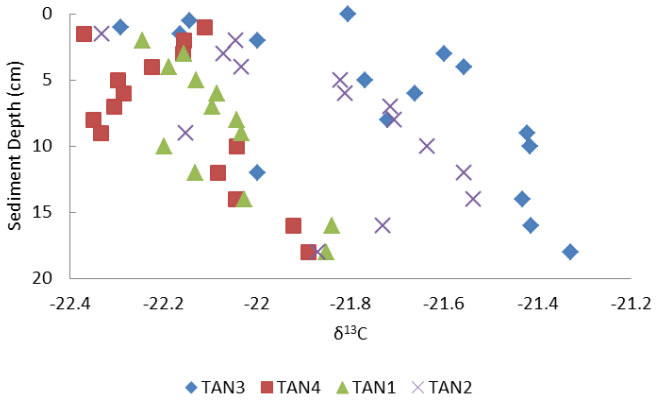

Figure 4.11.: Bulk δ^{13}C values for all analyzed cores.

ognizable. Instead, it is possible that the $U_{37}^{K'}$ has not been measured correctly, since the samples were first filtered prior to TEX_{86} analysis before analyzed for $U_{37}^{K'}$.

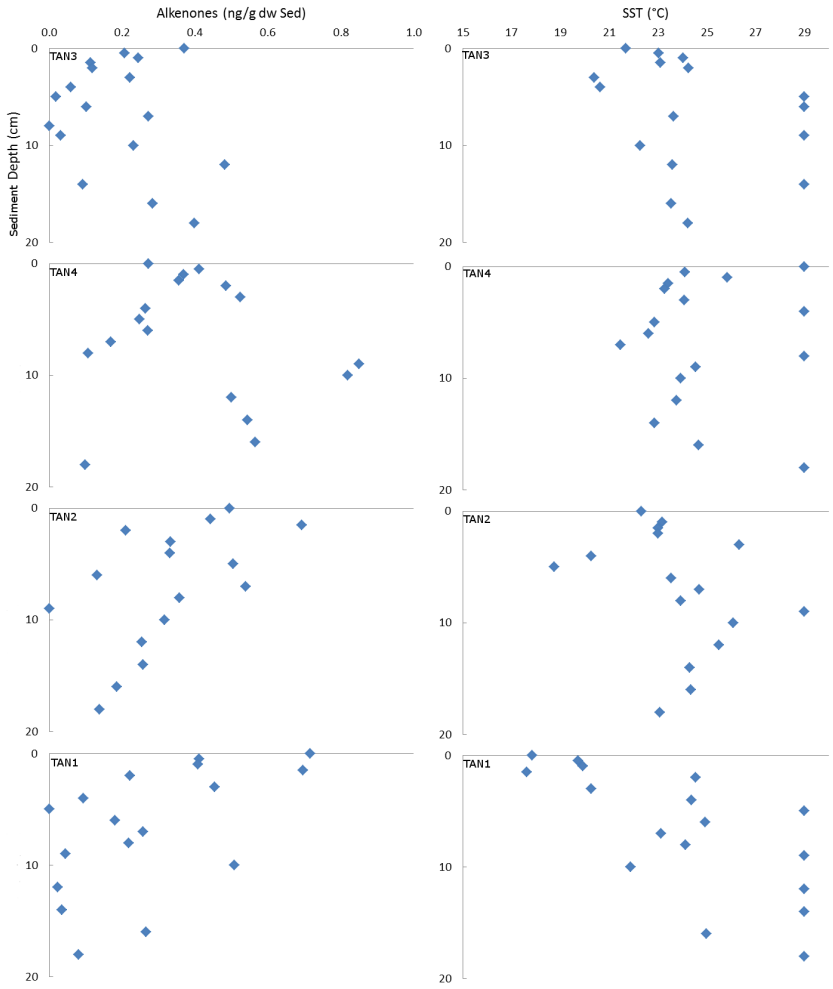

Figure 4.12.: Down core analysis of alkenone concentrations and $U_{37}^{K'}$ derived SST

4.2.3. GDGTs, BIT and TEX_{86}

TAN2 shows the lowest concentrations of branched GDGTs normalized to TOC, while it has the highest concentrations of isoprenoid GDGTs, ranging from $12\,\mu g/g$ to $498\,\mu g/g$ TOC (Tab. 4.1 and 4.2). TAN4 shows the lowest concentrations of isoprenoid GDGTs normalized to TOC, and TAN3 has the highest concentrations in branched GDGTs, ranging from $3\,\mu g/g$ to $6\,\mu g/g$ TOC. The isoprenoid GDGT concentrations in TAN3 and TAN4 are relatively constant and with $0.2\,\mu g/g$ comparatively low (Fig. 4.13). TAN2 and TAN1 show a decrease in concentrations with increasing core depth: from $0.9\,\mu g/g$ dw Sed down to $0.2\,\mu g/g$ dwt. Temperature reconstructions for TEX_{86}^{H} and TEX_{86}^{L} are relatively constant for each core, showing a temperature of 8.4 °C for TEX_{86}^{L} and 13 °C for TEX_{86}^{H} (Figure 4.13). TEX_{86}^{H} shows a shift towards colder temperatures from TAN3–TAN1. The temperature estimations of both proxies are similar in TAN1 and indicate a temperature of 12.5 °C. BIT shows constant values well below 0.1 in each core. Only TAN4 shows a slight increase in BIT with increasing depth, characterized by a BIT of 0.02 at the surface and 0.04 at the bottom of the core (Fig. 4.14).

Table 4.1.: Concentrations of isoprenoid GDGTs normalized to TOC (μg/g TOC), n.d. = not determined

	TAN3	**TAN4**	**TAN2**	**TAN1**
Sediment depth (cm)				
0	183			
0.5	218			
1	272	60		
1.5	382	60	437	
2	287	58	302	347
3	300	48	405	310
4	245	52	347	188
5	205	45	387	279
6	227	62	383	263
7	274	72	369	260
8	n.d	91	281	230
9	332	189	12	150
10	153	175	409	246
12	162	78	247	164
14	290	32	249	236
16	202	108	498	223
18	222	113	305	253

Table 4.2.: Concentrations of branched GDGTs normalized to TOC (μg/g TOC), n.d. = not determined

	TAN3	**TAN4**	**TAN2**	**TAN1**
Sediment depth (cm)				
0	3.2			
0.5	3.5			
1	4.7	0.7		
1.5	6.3	0.7	1.0	
2	5.3	0.6	0.7	3.4
3	5.4	0.6	1.0	3.1
4	4.4	0.7	0.9	1.9
5	3.2	0.6	1.0	2.8
6	4.0	0.9	1.0	2.7
7	4.8	1.0	0.9	2.7
8	n.d.	1.4	0.7	2.3
9	6.2	3.0	0.0	1.5
10	2.9	2.7	1.0	2.6
12	3.1	1.4	0.6	1.7
14	5.7	0.7	0.9	2.5
16	4.0	2.0	1.2	2.3
18	4.4	2.1	0.8	2.4

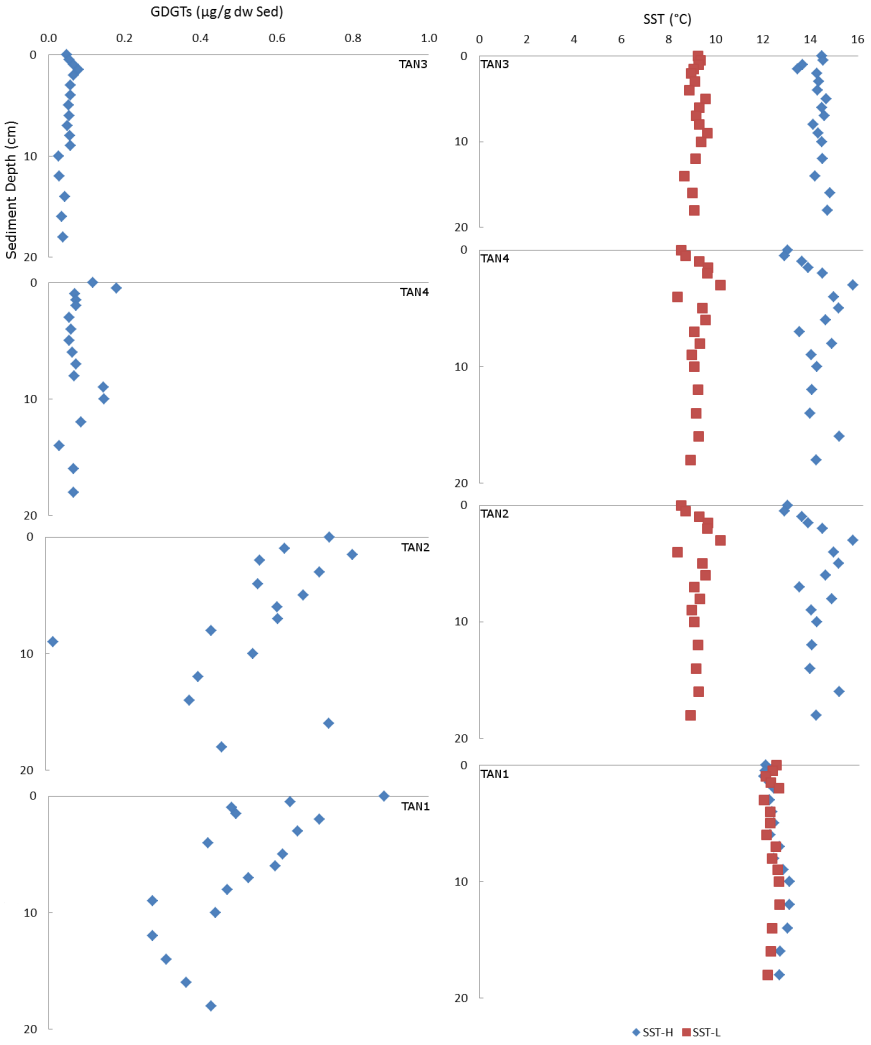

Figure 4.13.: Down core analysis of isoprenoid GDGT concentrations and TEX_{86}^{H} and TEX_{86}^{L} for all four cores

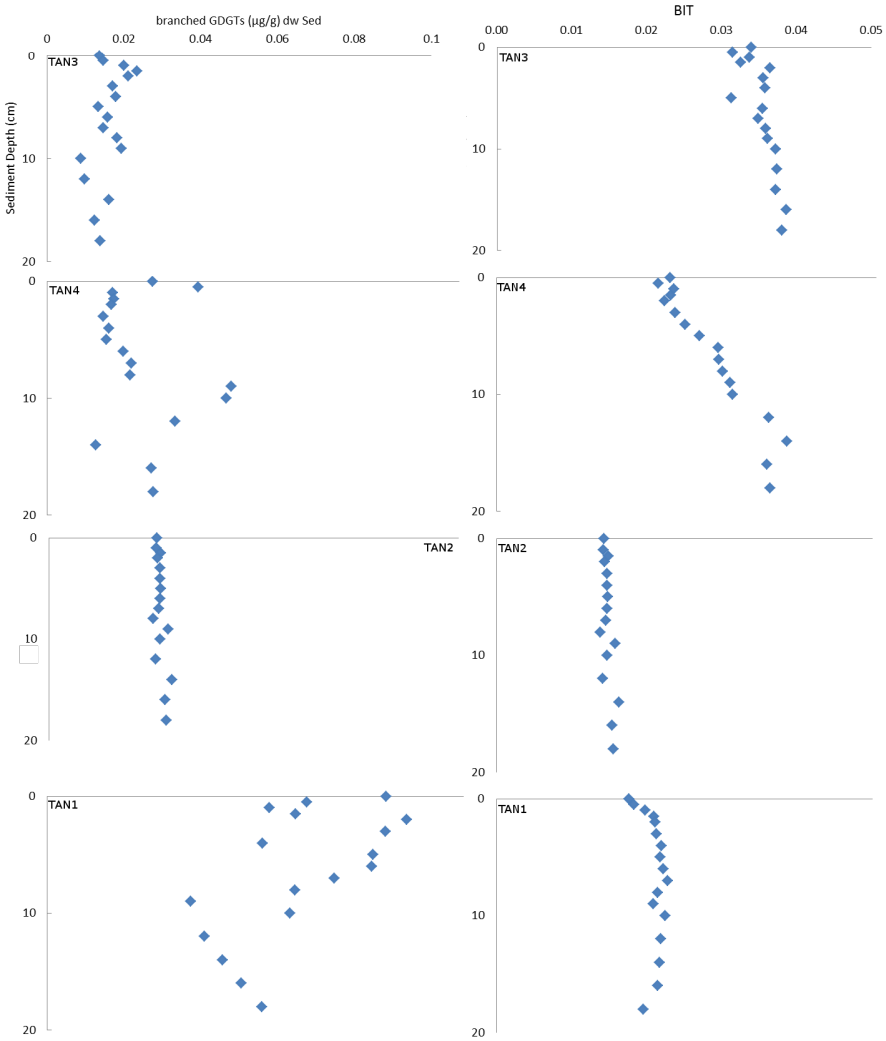

Figure 4.14.: Down core analysis of branched GDGT concentrations (μg/g) dw Sed and BIT

5. Discussion

5.1. Factors controlling organic carbon and biomarker concentrations

Figure 5.1 shows the oxygen concentrations for the transect. For the analyzed surface sediments it is generally observed that the concentrations of organic carbon, GDGTs and alkenones increase with water depth. This pattern could be related to changes in primary productivity. Figure 5.2 shows the thirty year record of chlorophyll-a concentrations off NE Japan. Although the Japanese east coast is affected by warm core rings (Mohiuddin et al., 2004) with increased chlorophyll levels, the chlorophyll concentrations are similar over the study area, with concentrations slightly higher at the coast ($1.18\,\mu g/l$) than at the open ocean site ($0.6\,\mu g/l$). This is a rather negligible difference and is unlikely to explain the high concentrations of biomarkers in off shore regions, in particular alkenones and TOC.

Instead, total organic carbon and biomarker concentration vary with oxygen concentrations (Figures 4.1, 4.3 and 4.5), i.e. high amounts of lipids and TOC have been measured where oxygen concentrations were low and decrease when bottom water oxygen concentrations rise. This is a typical observation when biomarkers are experiencing oxic degradation, and which has been reported by other studies (Lengger et al., 2012; Hoefs et al., 2002; Sinninghe Damsté et al., 2002). The lack of an age model and sedimentation rates make it difficult to evaluate the oxygen exposure time. Sedimentation rates could give an impression about the time that the organic matter is exposed to oxygen (oxygen

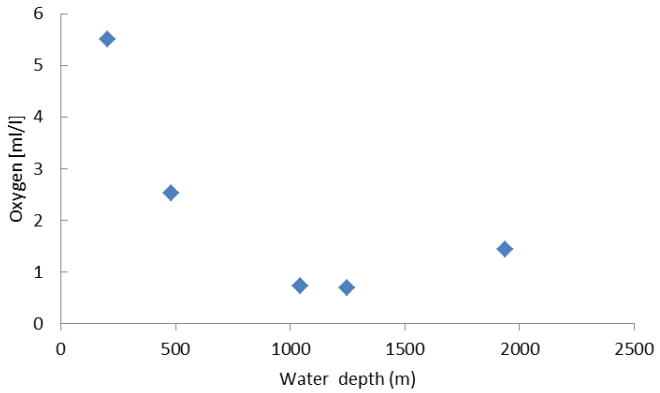

Figure 5.1.: Oxygen concentration in (ml/l) versus depth

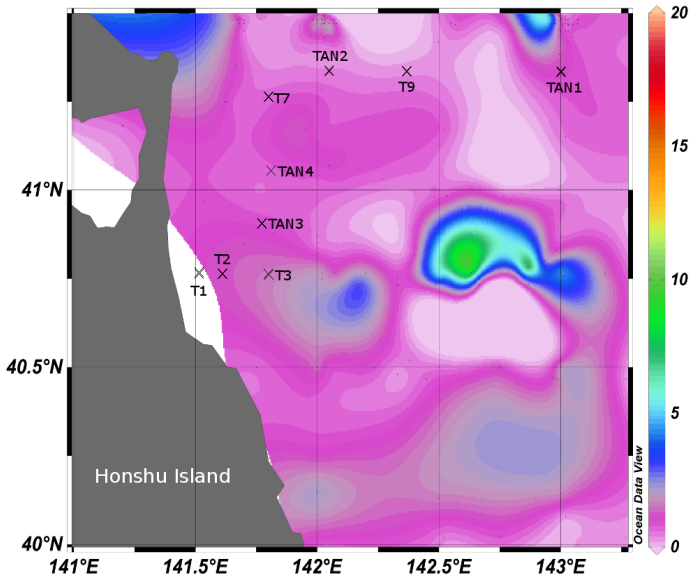

Figure 5.2.: Chlorophyll-a ($\mu g/l$) map, crosses indicate sampling stations (World Ocean Atlas, 2009)

exposure time) once it got deposited on the sea floor. The velocity of those rates determine the burial efficiency and thus how fast the organic matter is sealed off from oxic bottom waters and therefore from effective degradation. For example, a low sedimentation rate leads to a decreased burial efficiency and the organic matter is exposed longer to oxygen and thus is degraded for a longer time and faster than organic matter in environments with high sedimentation rates and anoxic bottom waters.

The source of the OM deposited on the sea floor is mainly of marine origin. This is reflected in the δ^{13}C values of circa -22‰ which represents the end member of marine surface sediments. Additionally, BIT is well below 0.1, which is typical for marine environments (Weijers et al., 2006b; Hopmans et al., 2004).

In order to assess the effects of oxic degradation, the preservation factor (Pf) has been calculated, according to (Hoefs et al., 2002).

$$Pf(\%) = \frac{[B]_{ox} * 2}{([B]_{unox.1} + [B]_{unox.2})} \tag{5.1}$$

where [B] is the concentration of a biomarker, $[B]_{unox.1/unox.2}$ = two unoxidized sample and $[B]_{ox}$ = oxidized sample. The unoxidized samples $[B]_{unox.1/unox.2}$ are represented by the surface sediments at 1046 m and 1938 m depth, based on the assumption that these are minor affected by oxic degradation. Table 5.1 shows the calculated Pfs for all stations and all analyzed biomarkers. Generally, two trends can be observed. The first trend is an decrease in preservation of biomarker with increasing oxygen concentrations. Second, a trend for the different component groups: GDGTs have lower preservation factors than alkenones. Inferred from ^{14}C analysis of alkenoens and GDGTs, Mollenhauer et al. (2008, 2007) attributes the age difference between crenarchaeol and alkenones to selective preservation. Alkenones, which are better preserved, show a higher ^{14}C age compared to the GDGTs. Similar conclusions were drawn by Kim et al. (2009a). Within the group of GDGTs it is observed that the branched GDGTs (I, II and III) have a higher preservation factor than the isoprenoid GDGTs, as previously

found by Huguet et al. (2008) in the oxic part of turbidites from the Madeira Abyssal Plain. Soil derived GDGTs are preserved to a larger degree than marine GDGTs and also degraded slower than the marine GDGTs. A seemingly higher preservation factor at high oxygen concentrations was calculated for GDGT-3 compared to GDGT-1,-2 and the crenarcheol regio isomer. Within the cores, isoprenoid GDGT concentrations are low for the shallow sampling sites. The cores located at the deeper sampling sites show higher concentrations (Figure 4.13). This trend is consistent with the observation for the surface sediments. The concentrations of branched GDGTs are always well below $0.1\,\mu g/g$ but increase with increasing water depth.

Table 5.1.: Preservation factor (Pf, in %) for isoprenoid GDGTs, branched GDGTs (I-III), alkenones and TOC in surface sediments. The Pf for each sample was calculated with 5.1.

	55m	**81m**	**105m**	**202m**	**482m**	**760m**	**1046m**	**1250m**	**1938m**
GDGT-0	2.8	3.0	10	14	45	65	199	137	200
GDGT-1	3.2	3.3	10	11	28	53	181	143	218
GDGT-2	2.9	3.2	8.7	10	26	51	175	150	225
GDGT-3	6.5	7.2	19	24	55	83	218	157	181
Crenarchaeol	3.9	3.8	12	15	43	62	217	155	182
Cren-isomer	2.5	2.6	7.4	10	24	50	193	163	206
I	4.9	3.6	7.9	37	62	67	208	195	191
II	19	11	24	38	63	72	188	157	211
III	16	10	21	27	65	70	193	158	206
TOC				31	162		200		182
$C_{37:3}$ **alkenone**	7.9	17	44	39	196	104	228	168	206
$C_{37:2}$ **alkenone**	14	28	59	44	202	102	238	177	182

5.2. Organic Proxies

5.2.1. $U_{37}^{K'}$

The sea surface temperature reconstructed with $U_{37}^{K'}$ shows an increased temperature of 5.5 °C over the first 100 m water depth compared to the 14.2 °C±0.6 that were reconstructed for the deeper located surface sediments (Fig. 4.4). The reconstructed temperature for the shallow depths does not match with todays sea surface temperature. The temperature difference corresponds to a shift of 0.11 units in the $U_{37}^{K'}$ index. This can have several reasons which will be discussed here.

One reason for the higher temperatures at shallow water depth can be due to warmer surface water temperatures on the shelf. This argument is comprehensible, since shallow waters warm faster than the deep oceans. However, neither the JODC temperature maps nor temperature maps of the World Ocean Atlas (2009) indicate higher temperatures close to the coast. Thus, differences in reconstructed temperatures due to warmer water masses on the shelf are unlikely. Another explanation for this phenomenon is the admixing of signals. The Kuroshio-Oyashio mixing front is a potential source of warmer $U_{37}^{K'}$ signals, since the Kuroshio Current transports warm (15 °C) waters from the south along the Japanese east coast. The mixing front moves to 41.5°N in December and during that time could deposit alkenones with a warmer signal. Against this theory speaks that the Kuroshio Current has a temperature of approximately 14 °C in December and the mixing front flows eastwards as part of the North Pacific gyre. Higher temperatures should then not only be recorded on the shelf but also at the other sampling stations. Thus, the mixing of warmer temperature signals derived from the Kuroshio Current can be ruled out. Mixing of warmer deeper sediment signals with cold surface temperature signals can also occur by bioturbation in the sediment. The burrowing activities of detrivores might mix recent alkenones with ancient alkenones and enhance oxygenation

of the sediment. In addition, the decomposition of organic matter by detrivores increases its surface area and with that enhances microbial degradation (Middelburg et al., 1993). Hypoxia reduces bioturbation in terms of reducing burrow length and depth. However, it is observed that some infauna remains active but due to low DO and decreased bioturbation oxygen, diffusion into the sediment is limited (Sturdivant et al., 2012). Over the first 100 m, DO concentrations of $5.5\,ml/l$ were measured, which corresponds to the range typical for oxic environments. Afterwards, concentrations decrease and oxygen diffuses not more than $5\,mm$ into the sediment (Fig. 5.3). Concentrations of $5.5\,ml/l$ and more would allow bioturbation by mesofauna and thus possibly upwards mixing of older sediments with warmer $U_{37}^{K'}$ signals. Since an oxygen profile for this depth is not available, bioturbation cannot be excluded. Unfortunately, the $U_{37}^{K'}$ record in the cores sheds no light on possible bioturbation, since it was not correctly measured (Fig. 4.12). However the downcore variation for TEX_{86} values (Fig. 5.4) are generally minor and especially for TAN3, recovered from a shallow station, almost constant. Another potential source of warm $U_{37}^{K'}$ values could be lateral transport of sediment from warmer areas. The lateral transport of alkenones off the coast of Honshu Island cannot be completely excluded since a sedimentological description of the cores is not available. Lateral transport is a common phenomenon described for alkenones (Benthien and Mueller, 2000; Kim et al., 2009a). The higher $U_{37}^{K'}$ values at shallow depths might be caused by lateral transport from warmer water regions, although temperature maps do not indicate such regions closeby. After excluding temperature differences, admixing of signals and to a certain extend lateral transport being the cause of higher $U_{37}^{K'}$ values at shallow depths, degradation is the last factor that can have an impact on the temperature signal. As discussed in section 5.1, dissolved oxygen concentrations are the only factor that have an influence on the compound concentrations at the different depths. A phenomenon related to oxic degradation is the preferential degradation of the $C_{37:3}$ alkenone (Hoefs et al., 1998b; Gong and Hollander, 1999; Huguet et al., 2009; Zabeti

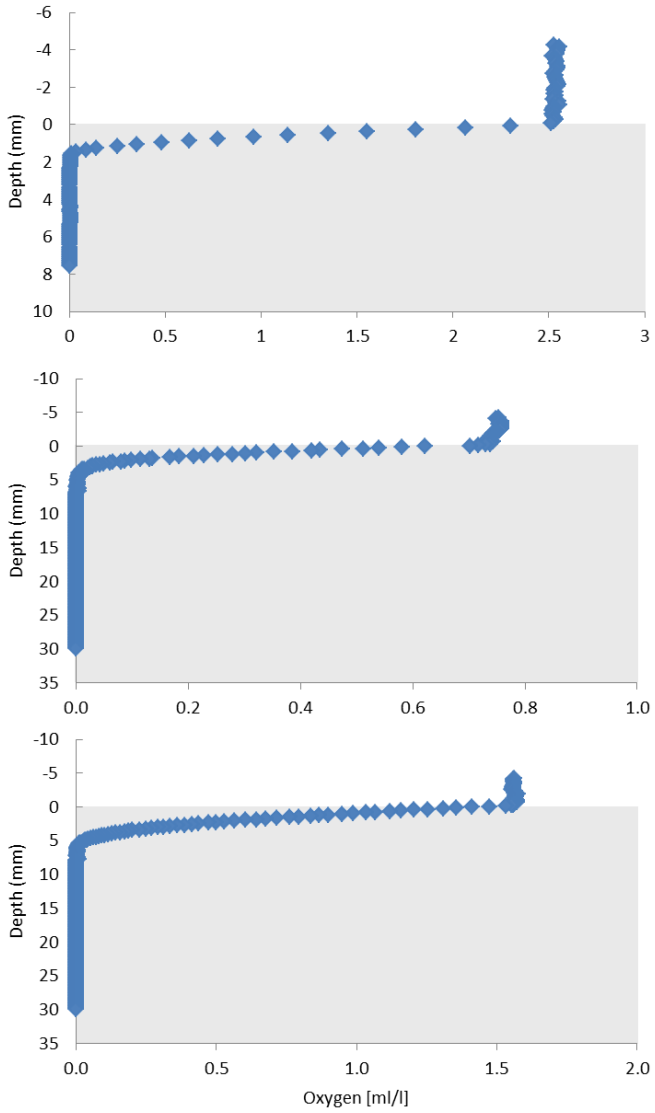

Figure 5.3.: Oxygen profiles for samples at 500m, 1000m and 2000m depth respectively. Negative depths indicate oxygen concentrations above the sediment-water interface. Courtesy K. Oguri, JAMSTEC.

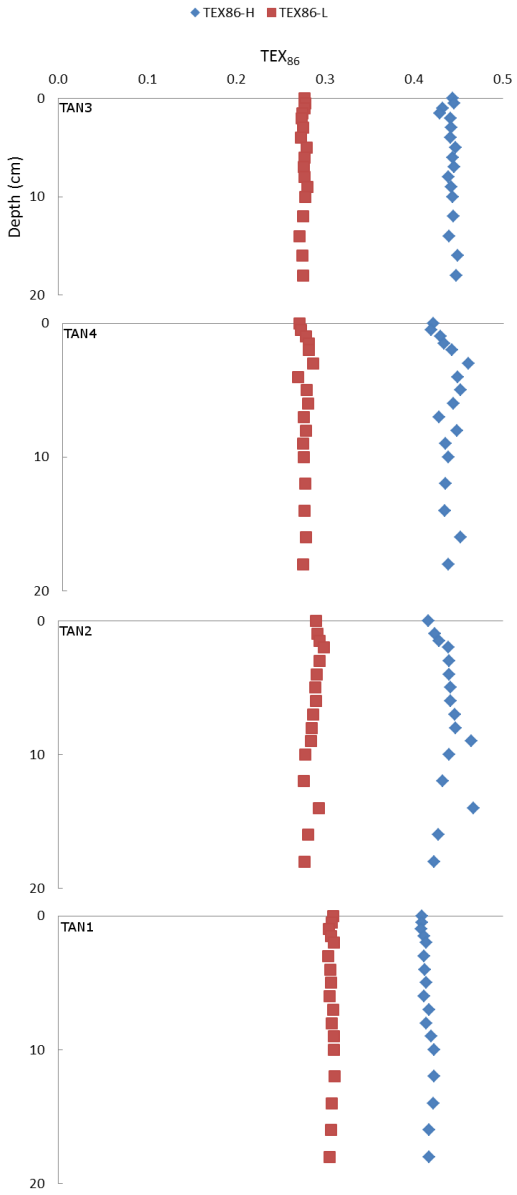

Figure 5.4.: Measured TEX_{86} values for cores TAN1-4, blue line represents TEX_{86}^{H}, the red line represents TEX_{86}^{L}

et al., 2010) although alkenones are very stable towards degradation compared to other compounds (Hoefs et al., 2002; Sinninghe Damsté et al., 2002). It is assumed, that the additional double bound leads to a higher reactivity of the $C_{37:3}$ than the $C_{37:2}$ alkenone. There is a little discrepancy about the impact of the preferential degradation: while Hoefs et al. (1998b) report an temperature offset of 5 °C, Gong and Hollander (1999); Huguet et al. (2009) estimates an offset of 2 °C to 2.5 °C compared to the reconstructed temperatures in the anoxic parts of their samples. The offset to the real temperature in this study is 5.5 °C warmer for the shallowest stations and fits with preferential degradation of $C_{37:3}$. The offset decreases to 3 °C and 2 °C warmer temperatures for the intermediate stations. Hoefs et al. (1998b) defined a degradation factor (DF) for alkenones to assess differences in degradation. In the equation, [B] again is the concentration of the biomarker, $[B]_{red}$ is an unoxidized sample, which again are represented by the sediment samples at 1046 m and 1938 m water depth, and B_{ox} is an oxidized sample. Table 5.2 shows an increased DF for $C_{37:3}$ over the first 100 m but then is equal to the DF $C_{37:2}$. All these findings indicate that the temperature offset of the $U_{37}^{K'}$ is caused by degradation.

$$DF = \frac{[B]_{red.}}{[B]_{ox.}}$$

Table 5.2.: Calculated degradation factor (DF) for alkenones

	T1	**T2**	**T3**	**TAN3**	**TAN4**	**T7**	**TAN2**	**T9**	**TAN1**
$C_{37:3}$	25	11	4	5	1	2	0.9	1	1
$C_{37:2}$	14	7	3	4	1	2	0.8	1	1

5.2.2. BIT

The BIT index is always well below 0.1 which is typical for marine environments, but is slightly higher in the oxic surface sediments (0.06) than in sub-

oxic sediments (0.01). Concentrations of branched GDGTs are high in areas with high soil input, i.e. close to river mouths from where the BIT decreases with increasing distance to the shore (Hopmans et al., 2004). For the surface sediments, decreasing BIT with increasing distance to the shore is observed, but since no rivers flow into the study area, increased BIT due to riverine input can be excluded. Another reason for increased BIT values is oxic degradation. Huguet et al. (2008, 2009) studied the effect of oxic degradation of soil organic matter in marine sediments and observed an increased preservation of soil derived GDGTs compared to the isoprenoid GDGTs. Calculating the preservation factor for oxidized and unoxidized parts of the turbidite reveals that branched GDGTs are an order of magnitude better preserved than crenarchaeol (Tab. 5.1, Fig. 4.8). Huguet et al. (2008) attributed this behavior to some form of matrix protection. The samples analyzed in this study show a similar behavior as described by Huguet et al. (2008, 2009). However, the BIT value does not rise as sharp as described for (Huguet et al., 2008), i.e. from 0.03 to 0.45. This has liekly to do with the lower oxygen exposure time. Thus, the increased BIT values are caused by the effect of oxic degradation.

5.2.3. TEX_{86}^{L}, TEX_{86}^{H}

Figure 4.7 shows the SST reconstructed with TEX_{86}^{H} and TEX_{86}^{L} respectively. The application of TEX_{86}^{H} yielded temperatures similar to contemporary SST, thus an impact of degradation can be excluded. This agrees with studies of Schouten et al. (2004) and Kim et al. (2009b), testing the stability of TEX_{86} towards oxic degradation by analyzing sediment cores from the Arabian Sea OMZ and incubation experiments. TEX_{86}^{L} underestimates the sea surface temperature by 2.5 °C to 6 °C over the first 1000 m water depth compared to the contemporary SST and TEX_{86}^{H}. Similar observations were reported by Wei et al. (2011) in the Southern Chinese Sea. TEX_{86} underestimated the SST by 4.3 °C to 9.2 °C for samples shallower than 100 m. In addition, the GDGT

composition at this depth differed from the composition of GDGTs from samples located >1000 m depth (Wei et al., 2011). This is likely due to a steady decrease for GDGT-3 below 500 m depth, while all other GDGTs remain relatively constant (Fig. 5.5, Tab. 5.1). A change in GDGT-3 concentrations will change the overall proportion of GDGTs to each other, which are needed for TEX_{86} calculations. TEX_{86}^{L}, in contrast to TEX_{86}^{H} might be substantially affected by this change, since it does not include GDGT-3 in the numerator as well as in the denominator. For this reason, the changes in the proportion can be displayed with the GDGT-2:GDGT-3 ratio.

$$\frac{[GDGT-2]}{[GDGT-2+GDGT-3]}$$

This ratio starts to increase at a depth of 500 m to 1000 m (Figure 5.6), which is the same depth range were GDGT-3 concentrations start to decrease. To examine if this changing ratio is a general phenomenon, the ratio was applied on the core tops of Kim et al. (2010) (Fig. 5.7), which shows the same change in proportion as for the sediment samples off Honshu Island. This phenomenon of changing GDGT-3 concentrations is related to depth rather than to the temperature, since those core tops cover a broad temperature range (Fig. B.1). Schouten et al. (2012) analyzed GDGTs as core lipids (CL) and intact polar lipids (IPL) in suspended particle matter (SPM) of the Arabian Sea over a depth range of 2000 m. Calculating the GDGT-2:GDGT-3 ratio for their data reveals the same pattern that has been found for the global core tops of Kim et al. (2010) (Fig. 5.8), showing that there is an increased GDGT-3 production in the water column. This signal disappears after approximately 1000 m, possibly due to admixing of differently produced GDGT ratios with increasing depth (Wei et al., 2011). This additional production of GDGT-3 is likely the cause for the ratio changes with depth. As a consequence, the offset between TEX_{86}^{L} and TEX_{86}^{H} and the offset between TEX_{86}^{L} and sea surface temperature will also change with depth. Thus, for the first 1000 m occurs an underestimation

for TEX_{86}^{L} derived SST. Beyond this depth, the temperature reconstruction fits in the range of contemporary SST. For past SST reconstructions, it should be considered that TEX_{86}^{L} SST are related to the water depth of the sediments, and TEX_{86}^{L} will underestimate the SST when the sediment samples are recovered from a depth range between 0 m to 1000 m. For this reason, TEX_{86}^{H} remains the reliable proxy for this study area, since it showed overall the best fit with todays sea surface temperature.

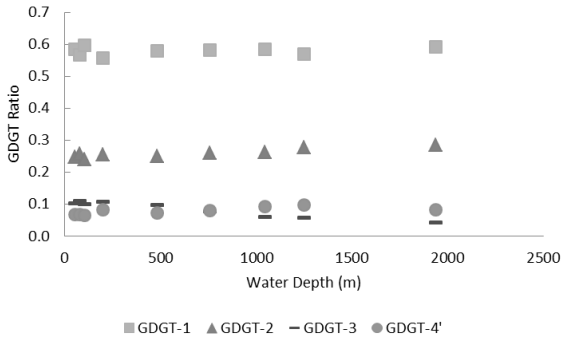

Figure 5.5.: Fractional abundance of TEX_{86} GDGTs changing with depth.

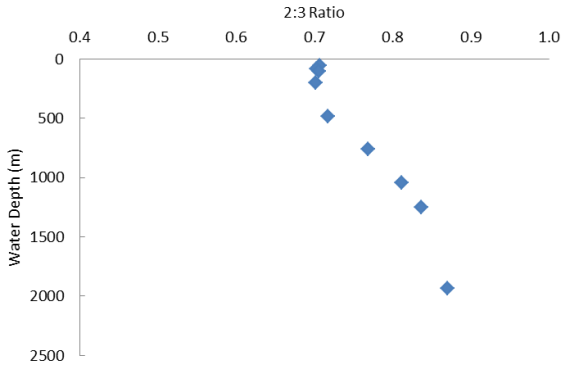

Figure 5.6.: GDGT-2:GDGT-3 Ratio calculated for all core tops off Honshu Island

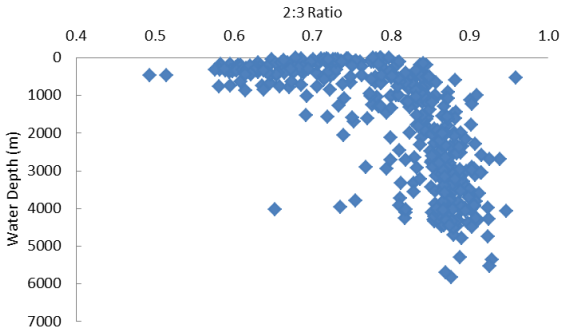

Figure 5.7.: GDGT-2:GDGT-3 Ratio calculated for all core tops used in Kim et al. (2010)

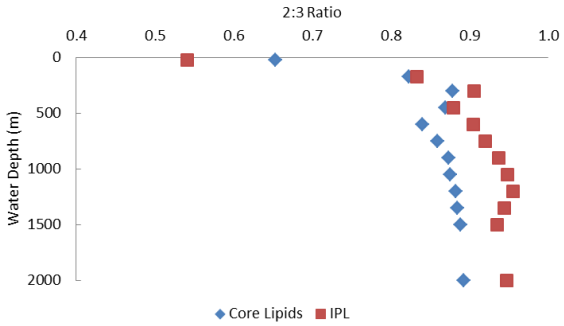

Figure 5.8.: The GDGT-2:GDGT-3 ratio in the water column plotted for the data of Schouten et al. (2012).

6. Conclusions

The organic carbon and biomarker concentrations in the surface sediments and in the core sediments follow the pattern of the oxygen concentrations, suggesting that oxygen concentrations have an influence on the biomarker concentration. These findings are in good agreement with other studies. For the biomarkers investigated in this study, the following order of relative resistance towards degradation can be established: TOC > alkenones > GDGTs, which is in agreement with other studies. Where surface sediments are exposed to increased bottom water oxygen concentrations and experience degradation, it is observed that $U_{37}^{K'}$ increases by 5.5 °C. Such rises in $U_{37}^{K'}$ are related to the preferential degradation of the $C_{37:3}$ alkenone. The small variations of the preservation factors suggest, that isoprenoid GDGTs are degraded at similar rates, thus there is no observed impact of degradation on the TEX_{86}^{H} record. The down core variations of TEX_{86} from different oxygen regimes are small as they fit contemporary temperatures. At the shallower depths, BIT values are slightly higher, which is a result of selective preservation of terrestrial organic matter in the marine realm. The higher preservation factors of branched GDGTs in comparison to isoprenoid GDGTs also suggest a slower degradation. The differential abundances of GDGT-3 at depths below and above 1000 m have implications for the TEX_{86}^{L} paleothermometry: this phenomenon can lead to an underestimation of sea surface temperatures if this proxy is applied at depths shallower than 1000 m, in this case up to 6 °C. TEX_{86}^{H} remains the more reliable proxy in this study area.

Since oxic degradation alters the distribution of lipids within one compound

class, biomarker ratios have to be applied with caution. The oxygenation history of the sampling area is necessary to know, especially for $U_{37}^{K'}$. In this study TEX_{86}^{H} seems to be stable towards oxic degradation.

Acknowledgments

I would like to thank Stefan Schouten and Gert-Jan Reichart a lot for their excellent supervision and the thesis topic, I think for everyone of us it contained loads of surprises! Furthermore thanks to Karoliina Koho for providing me with data and samples, Anchelique Mets, Jort Ossebar, Monique Verwij, Denise Dorhout and Kevin Donkers for the support in the lab, Jack Middelburg for helping me with my 'Master Plan', Ingrid Beekman for answering patiently all the questions I had. Another very special thank you to my parents for their moral and financial support. Thanks to the 'Rummikub-Club' for maintaining my sanity, to Yvonne, Tobi and Miri for being such good souls, to Sabine for decreasing my chances of being unemployed after graduation, to Lisa, Eli and Martina for the evenings with food, laughter, wine and dogs, Lennart 'heavily overrated moron' Groot, and last but not least, the pool full of very distinct characters making the BGC what it is. Thank you for the amazing year.

A. Abbreviations

ASE	Accelerated Solvent Extractor
BIT	Branched versus Isoprenoid Tetraethers
B/A	Bolling Allerod
DCM	Dichlormethane
DO	Dissolved Oxygen
EtoAc	Ethyl Acetate
GC	Gaschromatography
GC/MS	Gaschromatography/Mass spectrometry
GDGTs	Glycerol dibiphytanyl glycerol tetraethers
HPLC/MS	High pressure liquid chromatography/mass spectrometry
KTS	Korean/Tsushima Strait
LGM	Last Glacial Maximum
MAP	Madeira Abyssal Plain
MeOH	Methanol
NPIW	North Pacific Intermediate Water
OM	Organic Matter
SST	Sea Surface Temperature
$\mathbf{TEX}_{86}$	Tetraether Index of lipids with 86 carbons
TLE	Total Lipid Extract
TOC	Total Organic Carbon
TWC	Tsugaru Warm Current
$\mathbf{U}_{37}^{K'}$	Unsaturated Ketone Index
YD	Younger Dryas

B. Figures

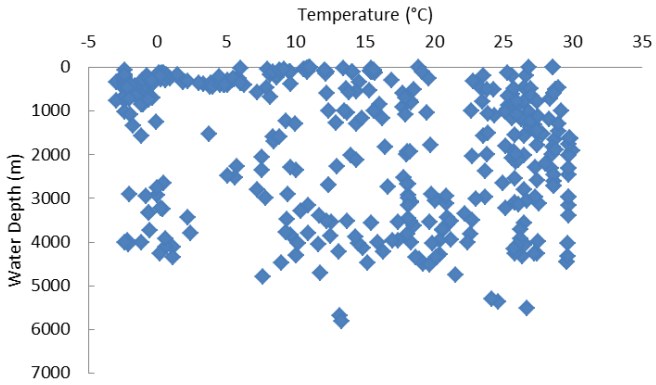

Figure B.1.: Water depth and temperature from core tops of Kim et al. (2010)

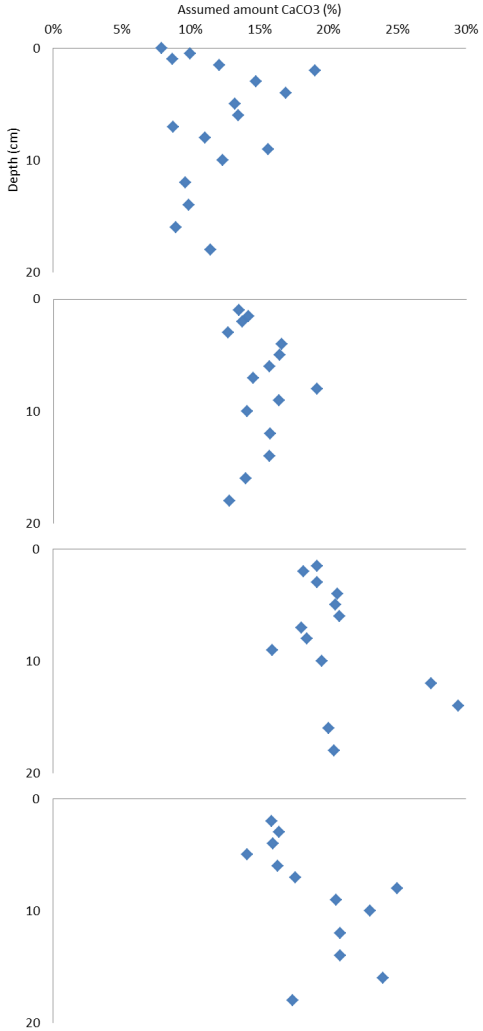

Figure B.2.: Down core variations of the maximum assumed $CaCO_3$ loss

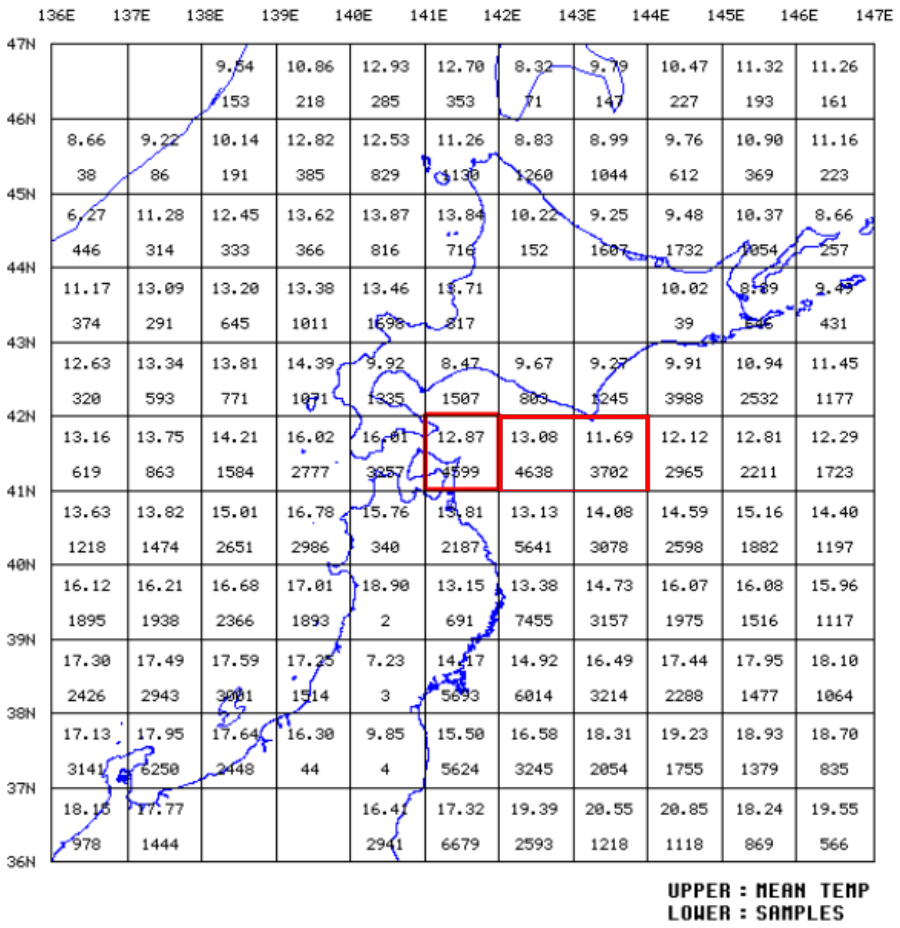

Latitude:**41.00N - 42.00N** Longitude:**141.00E - 142.00E**

Mean Temperature(deg C):**12.87** Number of Sample:**4599**
Max Temperature(deg C):**26.60** Standard Deviation:**6.25**
Min Temperature(deg C):**-2.10**

Figure B.3.: Statistics of annual sea surface temperature off Honshu Island in 1 degree mesh size, these temperatures were used in this report to compare them with the results of $U^{K'}_{37}$, TEX^{L}_{86} and TEX^{H}_{86}. (Japan Oceanographic Data Center)

Bibliography

Ahagon, N., Ohkushi, K., Uchida, M., and Mishima, T. (2003). Mid-depth circulation in the northwest Pacific during the last deglaciation: Evidence from foraminiferal radiocarbon ages. *Geophysical research letters*, 30.

Benthien, A. and Mueller, P. (2000). Anomalously low alkenone temperatures caused by lateral particulate and sediment transport in the Malvinas Current region, western Argentinian Basin. *Deep Sea Research Part I: Oceanographic Research Papers*, 47:2369–2393.

Brassel, S., Eglinton, G., Marlowe, I., Pflaumann, U., and Sarnthein, M. (1986). Molecular strategraphy: A new tool for climatic assessment. *Nature*, 320:129–133.

Chang, K.-I., Teague, W., Lyu, S., Perkins, H., Lee, D., Watts, D., Kim, Y., Mitchell, D., Lee, C., and Kim, K. (2004). Circulation and currents in the southwestern East/Japan Sea: Overview and review. *Progress in Oceanography*, 61:105–156.

de Leeuw, J., Rijpstra, W., and Schenk, P. (1981). The occurence and identification of C_{30},C_{31} and C_{32} alkan-15-one-1-diols in Unit I and Unit II Black Sea sediment. *Geochimica and Cosmochimica Acta*, 45:2281–2285.

Elderfield, H. and Ganssen, G. (2000). Past temperature and δ^{18}O of surface ocean waters inferred from foraminiferal Mg/Ca ratios. *Nature*, 405:442–445.

Ferreira, A., Miranda, A., Caetano, M., Baas, M., Vale, C., and Sinninghe Damsté, J. (2001). Formation of mid-chain alkane keto-ols by post-depostitional oxidation of mid-chain diols in Mediterranean sapropels. *Organic Geochemistry*, 32:271–276.

Gong, C. and Hollander, D. (1999). Evidence for differential degradation of alkenones under contrasting bottom water oxygen conditions: Implication for paleotemperature reconstruction. *Geochimica and Cosmochimica Acta*, 63:405–411.

Hagino, K., Okada, H., and Matsuoka, H. (2005). Coccolithophore assemblages and morphotypes of Emilana huxleyi in the boundary zone between the cold Oyashio and warm Kuroshio currents off the coast of Japan. *Marine Micropaleontology*, 55:19–47.

Harada, N., Ahagon, N., Sakamoto, T., Uchida, M., Ikehara, M., and Shibata, Y. (2006). Rapid fluctuations of alkenone temperature in the southwestern Okhotsk Sea during the past 120 kyr. *Global and Planetary Change*, 53:29–46.

Harada, N., Sato, M., Seki, O., Timmermann, A., Moossen, H., Bendle, J., Nakamura, Y., Kimoto, K., Okazaki, Y., Nagashima, K., Gobarenko, S., Ijiri, A., Nakatsuka, T., Menviel, L., Chikamoto, M., Abe-Ouchi, A., and Schouten, S. (2012). Sea surface temperature changes in the Okhotsk Sea and adjacent North Pacific during the last glacial maximum and deglaciation. *Deep-Sea Research II*, 61-64:93–105.

Hartnett, H., Keil, R., Hedges, J., and Devol, A. (1998). Influence of oxygen exposure time on organic carbon preservation in continental margin sediments. *Nature*, 391:572–574.

Hedges, J., Hu, F., Devol, A., Hartnett, H., Tsamakis, E., and Keil, R. (1999). Sedimentary organic matter preservation: A test for selective degradation under oxic conditions. *American Journal of Science*, 299:529–255.

Hedges, J., Keil, R., and Benner, R. (1997). What happens to terrestrial organic matter in the ocean? *Organic Geochemistry*, 27:195–212.

Herfort, L., Schouten, S., Boon, J., and Sinninghe Damsté, J. (2006). Application of the TEX86 temperature proxy to the southern North Sea. *Organic Geochemistry*, 37:1715–1726.

Hoefs, M., Rijpstra, W., and Sinninghe Damsté, J. (2002). The influence of oxic degradation on the sedimentary biomarker record I: Evidence from Madeira Abyssal Plain turbidites. *Geochimica and Cosmochimica Acta*, 666:2719–2735.

Hoefs, M., Sinninghe Damsté, J., de Lange, G., and de Leeuw, J. (1998a). Changes in kerogen composition across an oxidation front in Madeira Abyssal Plain turbidites as revealed by pyrolysis GC-MS. *Proceedings of the Ocean Drilling Programm, Scientific Results*, 157:591–607.

Hoefs, M., Versteegh, G., Rijpstra, W., de Leeuw, J., and Sinninghe Damsté, J. (1998b). Postdepositional oxic degradation of alkenones: Implications for the measurement of paleo sea surface temperatures. *Paleoceanography*, 13:42–49.

Hopmans, E., Weijers, J., Schefuss, E., Herfort, L., Sinninghe Damsté, J., and Schouten, S. (2004). A novel proxy for terrestrial organic matter in sediments based on branched and isoprenoid tetraether lipids. *Earth and Planetary Science Letters*, 224:107–116.

Hoshiba, M., Ahagon, N., Ohkushi, K., Uchida, M., Motoyama, I., and Nishimura, A. (2006). Foraminiferal oxygen and carbon isotopes during the last 34 kyr off northern Japan, northwestern Pacific. *Marine Micropaleontology*, 61:196–208.

Huguet, C., de Lange, G., Gustafsson, O., Middelburg, J., Sinninghe Damsté, J., and Schouten, S. (2008). Selective preservation of soil organic matter in

oxidized marine sediments (Madeira Abyssal Plain). *Geochimica and Cosmochimica Acta*, 72:6061–6068.

Huguet, C., Kim, J., de Lange, G., Sinninghe Damsté, J., and Schouten, S. (2009). Effects of long term oxic degradation on the $U^{K'}_{37}$, TEX_{86} and BIT organic proxies. *Organic Geochemistry*, 40:1188–1194.

Ikehara, K., Ohkushi, K., Shibahara, A., and Hoshiba, M. (2006). Change of bottom water conditions at intermediate depths of the Oyashio region, NW Pacific over the past 20000 yrs. *Global and Planetary Change*, 53:78–91.

Keigwin, L. (1998). Glacial-age hydrography of the far northwest Pacific. *Paleoceanography*, 13:323–339.

Killops, S. and Killops, V. (2005). *Introduction to Organic Geochemistry*. Blackwell Publishing.

Kim, J., Crosta, X., Michel, E., Schouten, S., Duprat, J., and Sinninghe Damsté, J. (2009a). Impact of lateral transport on organic proxies in the Southern Ocean. *Quarternary Research*, 71:246–250.

Kim, J., Huguet, C., Zonneveld, K., Versteegh, G., Roeder, W., Sinninghe Damsté, J., and Schouten, S. (2009b). An experimental field study to test the stability of lipids used for the TEX_{86} and $U^{K'}_{37}$ palaethermometers. *Geochimica and Cosmochimica Acta*, 73:2888–2898.

Kim, J., Schouten, S., Hopmans, E., Donner, B., and Sinninghe Damsté, J. (2008). Global sediment core-top calibration of the TEX86 paleothermometer in the ocean. *Geochimica and Cosmochimica Acta*, 72:1154–1173.

Kim, J., van der Meer, J., Schouten, S., Helmke, P., Willmott, V., Sangiorgi, F., Koc, N., Hopmans, E., and Sinninghe Damsté, J. (2010). New indices and calibrations derived from the distribution of crenarchaeal isoprenoid

tetraether lipids: Implications for past sea surface temperature reconstructions. *Geochimica and Cosmochimica Acta*, 74:4639–4654.

Lee, C. (1992). Controls on organic carbon preservation: The use of stratified water bodies to compare intrinsic rates of decomposition in oxic and anoxic systems. *Geochimica and Cosmochimica Acta*, 56:3323–3335.

Leider, A., Hinrichs, K., Mollenhauer, G., and Versteegh, G. (2010). Core-top calibartion of the lipid-based $U^{K'}_{37}$ and TEX_{86} temperature proxies on the southern Italien shelf (SW Adriatic Sea, Gulf of Taranto). *Earth and Planetary Science Letters*, 300:112–124.

Lengger, S., Hopmans, E., Reichart, G., Nierop, K., Sinninghe Damsté, J., and Schouten, S. (2012). Intact polar and core glycerol dibiphytanyl glycerol tetraether lipids in the Arabian Sea oxygen minimum zone. Part II: Selective preservation and degradation in sediments and consequences for the TEX_{86}. *Geochimica and Cosmochimica Acta*, http://dx.doi.org/10.1016/j.gca.2012.05.003.

Madureira, L., Conte, M., and Eglinton, G. (1995). Early diagenesis of lipid biomarker compounds in North Atlantic sediments. *Paleoceanography*, 10:627–642.

Menzel, D., Hopmans, E., van Bergen, P., de Leeuw, J., and Sinninghe Damsté, J. (2002). Development of photic zone euxinia in the eastern Mediterranean Basin during deposition of Pliocene sapropels. *Marine Geology*, 189:215–226.

Meyers, P. (1997). Organic geochemical proxies of paleoceanographic, paleolimnologic and paleoclimatic processess. *Organic Geochemistry*, 27:213–250.

Middelburg, J., Vlug, T., and van der Nat, F. (1993). Organic matter remineralization in marine systems. *Global and Planetary Change*, 8:57–58.

Müller, P., Kirst, G., Ruhland, G., von Storch, I., and Rosell-Mele, A. (1998). Calibration of the alkenone paleotemperature index $U_{37}^{K'}$ based on core-tops from the eastern South Atlantic and the global ocean (60°N-60°S). *Geochimica and Cosmochimica Acta*, 62:1757–1772.

Mohiuddin, M., Nishimura, A., Tanaka, Y., and Shimamoto, A. (2004). Seasonality of biogenic particle and planktonic foraminifera fluxes: response to hydrographic variability in the Kuroshio Extension, northwestern Pacific Ocean. *Deep Sea Research Part I: Oceanographic Research Papers*, 51:1659–1683.

Mollenhauer, G., Eglington, T., Hopmans, E., and Sinninghe Damsté, J. (2008). A radiocarbon-based assessment of the preservation characteristics of crenarchaeol and alkenones from continental margin sediments. *Organic Geochemistry*, 39:1039–1045.

Mollenhauer, G., Inthorn, M., Vogt, T., Zabel, M., Sinninghe Damsté, J., and Eglington, T. (2007). Aging of marine organic matter during cross-shelf lateral transport in the Benguela upwelling system revealed by compound specific-radiocarbon dating. *Geochemistry Geophysics Geosystems*, 8:doi:10.1029/2007GC001603.

Noda, A. and TuZino, T. (2010). Shelf-slope sedimentation during the late Quaternary on the southwestern Kruil frorearc margin, northern Japan. *Sedimentary Geology*, 232:35–51.

Nurnberg, D., Bijma, J., and Hemleben, C. (1996). Assessing the reliablility of magnesium in foraminiferal calcite as a proxy for water mass temperatures. *Geochimica and Cosmochimica Acta*, 60:803–814.

Oba, T., Irino, T., Yamamoto, M., Murayama, M., Takamura, A., and Aoki, K. (2006). Paleoceanographic change off central Japan since the last 144.000 years based on high-resolution oxzgen and carbon isotope records. *Global and Planetary Change*, 53:5–20.

Ohkouchi, N., Kawamura, K., Kawahata, H., and Okada, H. (1999). Depth ranges of alkenone production in the central Pacific Ocean. *Global Biogeochemical Cycles*, 13:695–704.

Ohkushi, K., Itaki, T., and Nemoto, N. (2003). Last Glacial-Holocene change in intermediate water ventilation in the Northwestern Pacific. *Quarternary Science Reviews*, 22:1477–1484.

Prahl, F., de Lange, G., Lyle, M., and Sparrow, M. (1989). Post-depositional stability of long-chain alkenones under contrasting redox conditions. *Nature*, 341:434–437.

Prahl, F., Muehlhausen, L., and Zahnle, D. (1988). Further evaluation of long-chain alkenones as indicators of paleoceanographic conditions. *Geochimica and Cosmochimica Acta*, 52:2303–2310.

Prahl, F. and Wakeham, S. (1987). Calibration of unsaturation patterns in long-chain ketone compositions for palaeotemperature assessment. *Nature*, 330:367–369.

Rampen, S., Willmott, V., Kim, J., Uliana, E., Mollenhauer, G., Schefuss, E., Sinninghe Damsté, J., and Schouten, S. (2012). Long chain 1,13- and 1,15-diols as potential proxy for paleotemperature reconstruction. *Geochimica and Cosmochimica Acta*, 84:204–216.

Schouten, S., Hopmans, E., Schefuss, E., and Sinninghe Damsté, J. (2002). Distributional variations in marine crenarchaeotal membrane lipids: a new tool for reconstructing ancient sea water temperatures? *Earth and Planetary Science Letters*, 204:265–274.

Schouten, S., Hopmans, E., and Sinninghe Damsté, J. (2004). The effect of maturity and depositional redox conditions on archaeal tetraether lipid paleothermometry. *Organic Geochemistry*, 35:567–571.

Schouten, S., Huguet, C., Hopmans, E., Kienhuis, M., and Sinninghe Damsté, J. (2007). Analytical Methodology for TEX_{86} Paleothermometry by High-Performance Liquid Chromatography/Atomospheric Pressure Cehmical Ionization-Mass Sectrometry. *Analytical Chemistry*, 79:2940–2944.

Schouten, S., Pitcher, A., Hopmans, E., Villanueva, L., van Bleijswijk, J., and Sinninghe Damsté, J. (2012). Intact polar and core glycerol dibiphytanyl glycerol tetraether lipids in the Arabian Sea oxygen minimum zone: I. Selective preservation and degradation in the water column and consequences for the TEX_{86}. *Geochimica and Cosmochimica Acta*, page http://dx.doi.org/10.1016/j.gca.2012.05.002.

Shackleton, N. (1982). The Deep-Sea Sediment Record of Climate Variability. *Prog. Oceanog.*, 11:199–218.

Shackleton, N. (1987). Oxygen isotopes, ice volume and sea level. *Quarternary Science Reviews*, 6:183–190.

Shibahara, A., Ohkushi, K., Kennett, J., and Ikehara, K. (2007). Late Quarternary changes in intermediate water oxygenation and oxygen minimum zone, northern Japan: A benthic foraminiferal perspective. *Paleoceanography*, 22.

Sikes, E., Nodder, T. O. S., and Volkman, J. (2005). Alkenone temperature records and biomarker flux at the subtropical front on the chatham rise, SW Pacific Ocean. *Deep-Sea Research Part 1*, 52:721–748.

Sinninghe Damsté, J., Hopmans, E., Pancost, R., Schouten, S., and Geenevasen, J. (2000). Newly discovered non-isoprenoid glycerol dialkyl glycerol tetraether lipids in sediments. *ChemComm*, DOI: 10.1039/b004517i.

Sinninghe Damsté, J., Rijpstra, W., Hopmans, E., Weijers, J., Overmann, B. F. J., and Dedysh, S. (2011). 13,16-Dimethyl Octacosanedioic Acid (iso-

Diabolic Acid), a Common Membrane-Spanning Lipid of Acidobacteria Subdivisions 1 and 3. *Applied and Environmental Microbiology*, 77:4147–4157.

Sinninghe Damsté, J., Rijpstra, W., and Reichart, G. (2002). The influence of oxic degradation on the sedimentary biomarker record II. Evidence from Arabian Sea sediments. *Geochimica and Cosmochimica Acta*, 66:2737–2754.

Sluijs, A., Schouten, S., Pagani, M., Woltering, M., Brinkhuis, H., Sinninghe Damsté, J., Dickens, G., Huber, M., Reichart, G., Stein, R., Matthiessen, J., Lourens, L., Pedentchouk, N., Backman, J., and Moran, K. (2006). Subtropical Arctic Ocean temperatures during the Palaeocene/Eocene thermal maximum. *Nature*, 411:610–613.

Sturdivant, S., Diaz, R., and Cutter, G. (2012). Bioturbation in a Declining Oxygen Environment, in situ Observations from Wormcam. *PLoS ONE*, 7:PLoS ONE 7(4): e34539. doi:10.1371/journal.pone.0034539.

Sun, M. and Wakeham, S. (1994). Molecular evidence for degradation and preservation of organic matter in the anoxic Black Sea Basin. *Geochimica and Cosmochimica Acta*, 58:3395–3406.

Teece, M., Getliff, J., Leftley, J., Parkes, R., and Maxwell, J. (1998). Microbial degradation of the marine prymnesiophyte Emiliania huxleyi under oxic and anoxic conditions as a model for early diagenesis: long chain alkadienes, alkenones and alkyl alkenoates. *Organic Geochemistry*, 29:863–880.

Versteegh, G., de Leeuw, J., Taricco, C., and Romero, A. (2007). Temperature and productivity influences on $U_{37}^{K'}$ and their possible relation to solar forcing of the Mediterranean winter. *Geochemistry Geophysics Geosystems*, 8:doi:10.1029/2006GC001543.

Versteegh, G., Janssen, J., de Leeuw, J., and Schneider, R. (2000). Mid-chain diols and keto-ols in SE Atlantic sediments: A new tool for tracing past sea surface water masses? *Geochimica and Cosmochimica Acta*, 64:1879–1892.

Volkman, J., Barrett, S., Dunstan, G., and Jeffrey, S. (1992). C_{30}-C_{32} alkyl diols and unsaturated alcohols in microalgae of the class Eustigmatophyceae. *Organic Geochemistry*, 18:131–138.

Warren, B. (1983). Why is no deep water formed in the North Pacific. *Journal of Marine Research*, 41:327–347.

Wei, Y., Wang, J., Liu, J., Dong, L., Li, L., Wang, H., Wang, P., Zhao, M., and Zang, C. (2011). Spatial Variations in Archaeal Lipids of Surface Water and Core-Top Sediments in the South China Sea and Their Implications for Paleoclimate Studies. *Applied and Environmental Microbiology*, 77:DOI:10.1128/AEM.00580–11.

Weijers, J., Schouten, S., Hopmans, E., Geenevasen, J., David, O., Coleman, M., Pancost, R., and Sinninghe Damsté, J. (2006a). Membrane lipids of mesophilic anaerobic bacteria thriving in peats have typical archaeal traits. *Environmental Microbiology*, 8:648 – 657.

Weijers, J., Schouten, S., Spaargaren, O., and Sinninghe Damsté, J. (2006b). Occurrence and distribution of tetraether membrane lipids in soils: Implications for the use of the TEX_{86} proxy and the BIT index. *Organic Geochemistry*, 37:1680–1693.

Weijers, J., Steinmann, P., Hopmans, E., Schouten, S., and Sinninghe Damsté, J. (2011). Bacterial tetraether membrane lipids in peat and coal: Testing the MBT-CBT temperature proxy for climate reconstruction. *Organic Geochemistry*, 42:477–486.

Wuchter, C., Schouten, S., Wakeham, S., and Sinninghe Damsté, J. (2005). Temporal and spatial variation in tetraether membrane lipids of marine Crenarchaeota in particulate organic matter: Implications for TEX_{86} paleothermometry. *Paleoceanography*, 20:doi:10.1029/2004PA001110.

Wuchter, C., Schouten, S., Wakeham, S., and Sinninghe Damsté, J. (2006). Archaeal tetraether membrane lipid fluxes in the northeastern Pacific and the Arabian Sea: Implications for TEX_{86} paleothermometry. *Paleoceanography*, 21:doi:10.1029/2006PA001279.

Yamamoto, M., Shimamoto, A., Fukuhara, T., Naraoka, H., Tanaka, Y., and Nishimura, A. (2007). Seasonal and depth variations in molecular and isotopic alkenone composition of sinking particles from the western North Pacific. *Deep-Sea Research I*, 54:1571–1592.

Yamamoto, M., Shimamoto, A., Fukuhara, T., Tanaka, Y., and Ishizaka, J. (2012). Glycerol dialkyl glycerol tetraether and TEX_{86} index in sinking particles in the western North Pacific. *Organic Geochemistry*, http://dx.doi.org/10.1016/j.orggeochem.2012.04.010.

Yasuda, I., Okuda, K., and Shimizu, Y. (1996). Distribution and Modification of North Pacific Intermediate Water in the Kuroshio-Oyashio Interfrontal Zone. *Journal of Physical Oceanography*, 26:448–465.

Zabeti, N., Bonin, P., Volkman, J., Jameson, I., and Rontani, J. (2010). Potential alteration of $U_{37}^{K'}$ paleothermometer due to selective degradation of alkenones by marine bacteria isolated from the haptophyte Emiliana huxleyi. *FEMS Microbiology Ecology*, 73:83–94.

Zachos, J., Bohaty, S., John, C., McCarren, H., Kelly, D., and Nielsen, T. (2007). The Paleocene-Eochene carbon isotope excursion: constraints from individual shell planktonic foraminifer records. *Phil. Trans. R. Soc. A*, 365:1829–1842.

Zachos, J., Roehl, U., Schellenberg, S., Sluijs, A., Hodell, D., Kelly, D., Thomas, E., Nicolo, M., Rafi, I., Lourens, L., McCarren, H., and Kroon, D. (2005). Rapid acidification of the ocean during the Paleocene-Eocene Thermal Maximum. *Science*, 308:1611–1615.